ACS Infectious Diseases

pubs.acs.org/journal/aidcbc

Article

Temporal Effects of a Viral Peptide on Glucose-Stimulated Insulin Secretion

Firdos Firdos,[†] Tapabrata Pramanik,[†] and Aditya Mittal*

Cite This: *ACS Infect. Dis.* 2025, 11, 1167−1179

Read Online

ACCESS | Metrics & More | Article Recommendations | Supporting Information

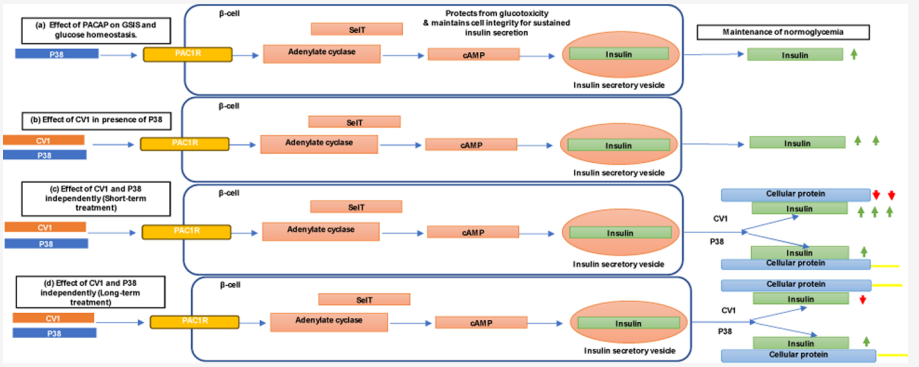

ABSTRACT: Impaired glucose homeostasis, often attributed to the destruction of insulin-secreting pancreatic β-cells, results in Type 1 diabetes (T1D). While both genetic and environmental factors have been implicated in the onset of T1D, there is an increase in clinical observations of T1D resulting from or triggered by viral infections. Despite the increase mentioned above, mechanistic insights into viral-induced T1D onset remain scarce. The key question of how viral infections may impact insulin secretion, thereby affecting glucose-stimulated insulin secretion (GSIS), is still unanswered. In this work, we correlate GSIS and viral peptides for the first time. Using the Mouse Insulinoma 6 (MIN6) cell line as a model system for β cells, we studied pituitary adenylate cyclase-activating polypeptide (PACAP) potentiated GSIS. Specifically, we noted that two forms of PACAP, namely, PACAP38 (P38) and PACAP27 (P27) are important in GSIS. From proteomes of chikungunya and dengue viruses (CHIKV and DV, respectively) implicated in triggering T1D, we identified viral peptides that were similar (but not identical) to PACAP. We report that a peptide from CHIKV, termed as CV1, enhances insulin secretion in MIN6 cells along with P38; however, independent treatments with CV1 yield variable outcomes based on duration of incubation. While short-term treatment shows viral peptides outcompeting P38, leading to increased insulin secretion without cytotoxicity, there is a decrease in cell viability with longer incubations under some conditions. Remarkably, long-term CV1 incubation significantly reduces glucose sensitivity of and GSIS by MIN6 cells. We report the first experimental evidence linking viral peptides to GSIS (specifically PACAP-stimulated).

KEYWORDS: *GSIS, MIN6, PACAP, viral peptides, molecular mimicry, Type 1 diabetes*

Classically, Type 1 diabetes (T1D) is the disruption of glucose homeostasis because of the destruction of insulin-secreting β-cells within the pancreatic islets responsible for insulin secretion. It is usually referred to as insulin-dependent diabetes due to the low insulin levels in the affected patients, which distinguishes it from Type 2 diabetes (T2D), the insulin-resistant category.[1] In 2014, the American Diabetes Association further categorized T1D into Type 1A and Type 1B. While Type 1A is caused by an autoimmune response, Type 1B or idiopathic diabetes cases exhibit the same symptoms without any evidence of autoimmunity.[1,2] While constituting only 5−10% of all diabetic cases, T1D gives rise to significant complications, including vascular diseases, alongside enduring physiological issues with far-reaching implications.[2,3] Among environmental agents, viral infections have been notably associated with both induction and enhancement of T1D. Several studies have reported sync in the pattern of T1D onset and season of viral infections.[4] Isolation of viruses from pancreatic tissue samples of diagnosed T1D patients further establishes the association of viral infection and T1D.[5−7] The correlation between T1D induction and enterovirus (EV) infections is the most robust, with supportive evidence from both clinical and molecular studies.[8] Apart from EV, chikungunya, herpesvirus, influenza virus, parechovirus,

Received: December 19, 2024
Revised: April 9, 2025
Accepted: April 15, 2025
Published: April 24, 2025

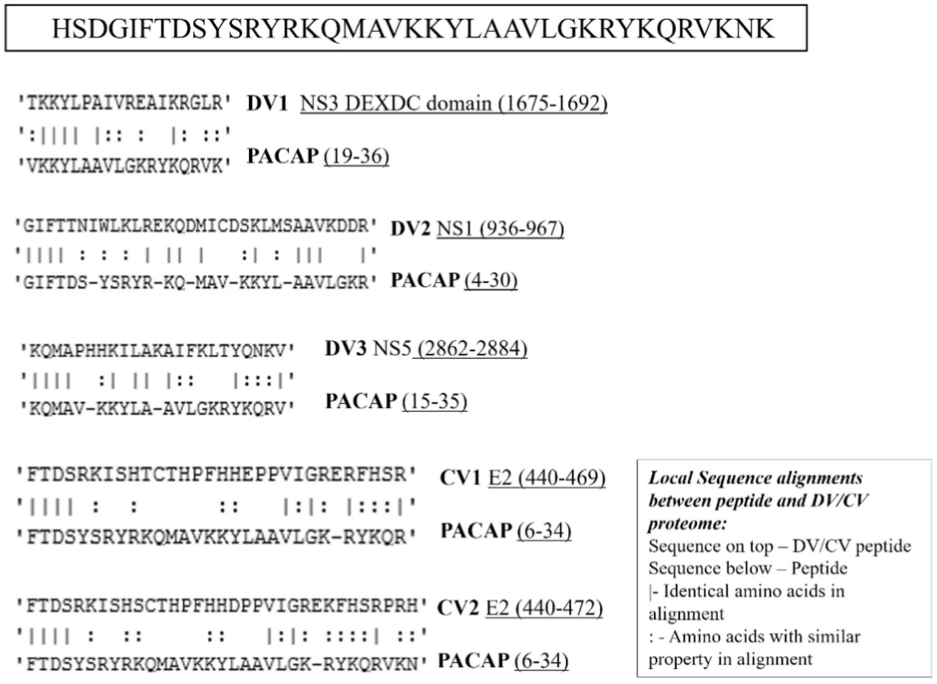

Figure 1. A local sequence alignment was performed on the proteomes of dengue and chikungunya viruses against PACAP38 using the LALIGN function in MATLAB. Viral peptides that contained a continuous stretch of four identical residues were selected. The screening of the results revealed five viral peptides, three from dengue virus (DV) and two from chikungunya virus (CV), aligned with PACAP38.

rotavirus, mumps, and rubella viruses have also been known to bear a potential pathogenic role in causing T1D.[4,9] Epidemiological reports have shown a relationship between severe dengue fever and diabetes,[10] as well as acute pancreatitis.[11] An epidemiological case report associating acute chikungunya virus infection and subsequent diabetic ketoacidosis (DKA) in a Type 1 diabetic patient has also been reported.[12] Three possible mechanisms have been implicated in virus-induced T1D pathogenesis—(a) virus persistence, (b) bystander activation, and (c) molecular mimicry.[13] After a viral infection, viral peptides may enter the bloodstream following the lytic cycle. This lytic mixture could contain floating viral particles (premature or mature virions) that can travel through the circulating blood in the body. These viral particles and their proteins, which may mimic the hormones and proteins of the host body, can lead to either activation or inhibition of the signaling pathways that are essential for host cell functions.[14] Here, we propose an alternate consequence of molecular mimicry, wherein the viral mimic may show synergistic or competitive binding with the host peptide-receptor, thereby altering its function.

Insulin secretion is a complex process tightly regulated by the plasma glucose levels in the system. Glucose acts via a diverse network (neural circuits, hormones, and other nutrients) to induce the time-tuned GSIS in pancreatic β-cells.[15,16] In addition to glucose, other factors can also influence insulin secretion. For example, amino acids derived from protein digestion, certain gastric hormones (e.g., incretins such as glucagon-like peptide-1 or GLP-1 and PACAP), and neural signals can enhance or modulate GSIS.[17] These factors can either directly affect the beta cells or indirectly influence their function by various signaling pathways[15,18] through the help of G protein-coupled receptors (GPCR).[19] PACAP is one of the inducers of adenylate cyclase and participates in various regulatory signaling processes as an important ligand for the GPCR receptor, PAC1R. PACAP plays a crucial role in various signaling reactions within the nervous system, thyroid gland, reproductive system, adrenal gland, digestive tract, liver, respiratory tract, cardiovascular system, and pancreas.[20,21] The biologically active forms of pituitary adenylate cyclase-activating polypeptide (PACAP) family, PACAP38 (P38) and PACAP27 (P27), are recognized for their potent ability to stimulate insulin secretion.[22] Experimental studies on PACAP knockout models and transgenics provide robust evidence of their involvement in GSIS.[23,24] In this study, we screened the chikungunya virus (CHIKV) and dengue virus (DV) proteomes for similarity against insulin and PACAP family members. Based on primary sequence similarity, CHIKV and DV peptide mimics were identified for PACAP. Intervening any of these mechanisms of PACAP-heightened insulin secretion due to PACAP mimicking viral peptides may result in insufficient or decreased insulin levels and disruption of glycemic control, thus leading to the T1D condition. Our research utilizes the well-established pancreatic β-cell model system MIN6 cell line to study GSIS.[25,26] While MIN6 is a widely used beta-cell model, extension of the current work with primary pancreatic islets or in vivo models that are considered more physiologically relevant would allow application of our results to clinical settings. Interestingly, the "honeymoon phase" in T1D is a well-known period of partial recovery after diagnosis, reducing the dependence on external insulin. The duration of the T1D honeymoon phase varies widely, with some patients remaining insulin-independent for up to 7 years[27−29] These studies provide ample evidence to establish the temporal nature of T1D—a clinical observation that we have managed to observe with MIN6 cells. In conjunction with the available literature, our results open the avenue for viewing T1D and its temporality as a possible consequence of viral peptides mimicking PACAP and influencing its physiological action.

https://doi.org/10.1021/acsinfecdis.4c01025
ACS Infect. Dis. 2025, 11, 1167−1179

RESULTS AND DISCUSSION

Screening of Viral Peptides. Based on the screening of a stretch of four continuous identical amino acids in the CHIKV−P38 and DV-P38 alignments and the identity and coverage criteria of the viral peptides, we obtained two CHIKV (CV1, CV2) and three DV peptides (DV1, DV2, and DV3) for further analysis in Figure 1. The two CHIKV peptides (CV1, CV2) spanned the region from the E2 protein of the virus, respectively, while the DV peptides (DV1, DV2, DV3) aligned against the NS3, NS1, and NS5 proteins of the virus. Out of all these 5 peptides, we have chosen CV1 for experimental studies with PACAP based on its lowest binding energy (kcal/mol) with the PAC1 receptor, as explained in further results. Peptides and their sequences are given in Supporting Information Table S1.

Selection of Host PACAP Peptides for Positive Control. The CABS-dock protocol for protein−peptide docking was used for the prediction of PAC1R-peptide complexes.[30] We chose the CABS-dock protocol for its accuracy in predicting peptide−protein interactions without requiring an initial peptide structure, offering flexibility and reliable results. Since the CABS-dock protocol is based on coarse grain force field predictions, a more robust MM/PBSA approach was applied for the deduction of the binding free energy of the protein-peptide complex. Two positive controls were selected for comparison against viral peptide complexes. One was the physiological form of PACAP, P27, and the other was selected from the list of 28-mer PACAP variants docked against PAC1R. Out of the 11 models, PACAP (10−37) docked against PAC1R exhibited the highest binding affinity and was selected as the second positive control (Table 1).

Table 1. Binding Free Energy Deduction of the Positive Control Peptides P27 and P38 with the PAC1R Receptor by MM/PBSA[a]

PACAP peptides	binding free energy (kcal/mol)
PACAP27*	−28.947 ± 5.0327
1−28 *aa*	−28.228 ± 5.3992
2−29 *aa*	−29.812 ± 5.2623
3−30 *aa*	−10.915 ± 4.1400
4−31 *aa*	−29.101 ± 4.5704
5−32 *aa*	−22.843 ± 4.7729
6−33 *aa*	−19.480 ± 4.9008
7−34 *aa*	−27.176 ± 6.0762
8−35 *aa*	−25.613 ± 5.0560
9−36 *aa*	−30.142 ± 5.0906
10−37 *aa**	**−43.8753 ± 5.8063**
11−38 *aa*	−15.5886 ± 3.6126

[a]**Note:** The one marked with the "*" has been selected as a positive control.

Identification of Potential Molecular Mimics of PACAP. In comparison to P27, CV1, DV2, and DV3 exhibited a lower binding free energy and dissociation constant (Table 2). The respective data and additional information for Table 2 are provided in Supporting Information Table S2. The second positive control of P38 (10−37) had a lower dissociation constant and binding energy than all the viral peptides but showed maximum proximity to dissociation constants of CV1, DV2, and DV3. The dissociation constant values indicate that under increased viral load, the five viral peptides, especially,

Table 2. Binding Free Energy and Dissociation Constant of DV and CV Peptides with PAC1R[a,b]

control	viral peptide	binding free energy of viral peptide bound to PAC1R (kcal/mol)	K_d (viral peptide)/K_d(control)
PACAP27	**DV1**	**−17.046**	**5.76×10^{8}**
	DV2	**−36.6392**	**2.18×10^{-06}**
	DV3	**−34.1693**	**1.43×10^{-04}**
	CV1	**−40.8629**	**1.69×10^{-09}**
	CV2	**−19.3724**	**1.12×10^{7}**
PACAP (10−37)	**DV1**	**−17.046**	**5.61×10^{19}**
	DV2	**−36.6392**	**2.12×10^{5}**
	DV3	**−34.1693**	**1.39×10^{7}**
	CV1	**−40.8629**	**1.65×10^{2}**
	CV2	**−19.3724**	**1.09×10^{18}**

[a]These values are lower in comparison to P27 and similar to P38 (residues 10−37). [b]Note: Subsequently, further wet experiments were conducted using P38 (control), CV1 (treatment), and a random viral peptide that does not share any similarities with the peptides, referred to as NC (negative control).

CV1, DV2, and DV3, bear the potential to act as competitive binders against the host PACAP. Therefore, these five peptides may act as potential molecular mimics to affect PACAP functioning during CHIKV or DV infection. The comparison of contact maps of the host PACAP and viral peptides docked against PAC1R shows an extensive overlap with respect to the residues on the binding interface of the receptor. The residue Glu104 of PAC1R is known to be crucial for ligand binding, and its mutation reduces the binding of PACAP38.[31] The presence of this residue in the contact maps of viral peptide-PAC1R complexes further enhances the potential of these peptides as molecular mimics. The residues of PAC1R that bind to both control and viral peptides are given in Table S3. The critical residues of PACAP for PAC1R contacts are identified and detailed in this table. This table provides a comprehensive list of the key interactions.

In our wet experimental studies, P38 was selected as the positive control. CV1, a peptide derived from the E2 protein of chikungunya virus, was selected due to its significant similarity to PACAP and its high binding affinity to PAC1R, comparable to the control peptide PACAP. While the computational results made CV1 the first candidate to assess the impact of viral peptides on GSIS, it is important to appreciate that protocols set up with CV1 could be made directly applicable for other peptides of interest. Importantly, PACAP was used as a positive control, and a (scrambled) viral peptide dissimilar to other peptides was randomly selected and used to serve as a negative control (NC). Secretion data were normalized to the negative control NC250, used as a blank, to evaluate the effects of different conditions under high glucose. We have included the absolute standardization values in terms of picomol/mg of insulin for insulin ELISA corresponding to 0 nM P38 or NC 250 nM to express the percent change in insulin secretion. These values correspond to a 100% level of insulin secretion, as mentioned in Tables S4−S7 and S10, respectively. This approach facilitated an effective comparison of results with P38 and CV1 across all experimental sets without interference of noise and variation for independent replicates.

Standardization of P38. First, we standardized and assessed insulin secretion using our control peptide, P38. We

https://doi.org/10.1021/acsinfecdis.4c01025
ACS Infect. Dis. 2025, 11, 1167−1179

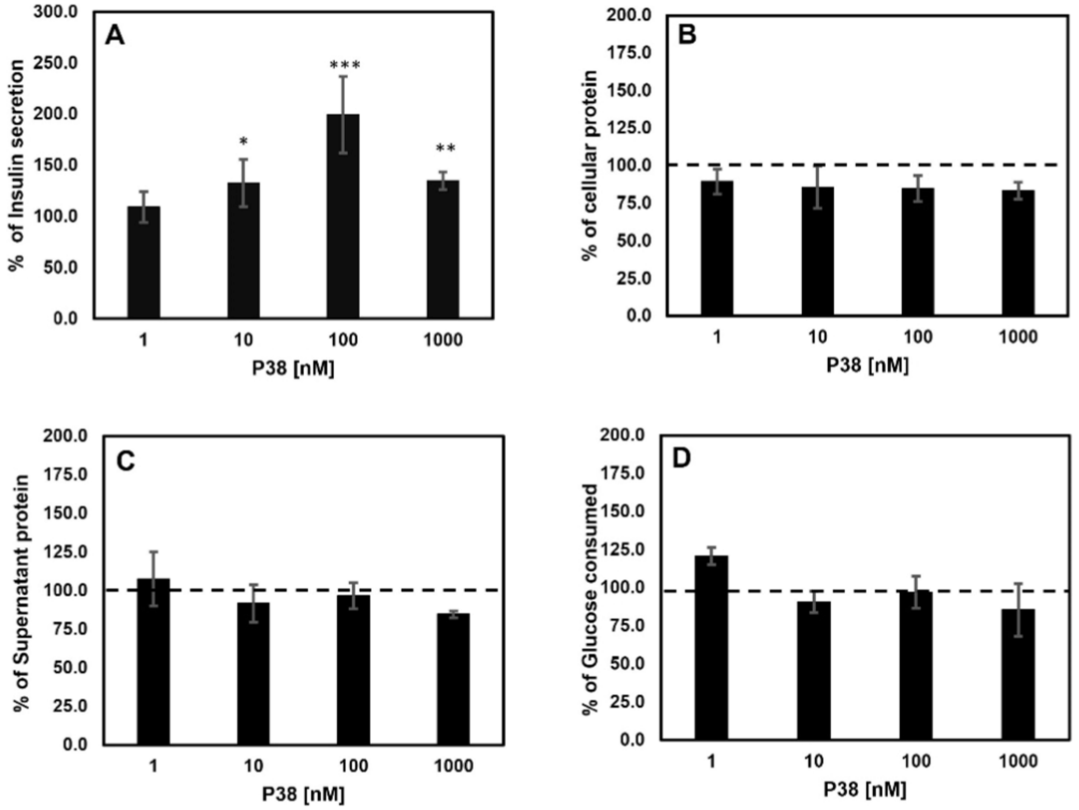

Figure 2. (A) Demonstrates increasing insulin secretion at 25 mM glucose with varying P38 concentrations. The values include SEM ± mean (n = 4, triplicate), and p-values are indicated as * $p < 0.05$, ** $p < 0.01$, and *** $p < 0.001$. Figure 2B and C depicts cellular and supernatant proteins, while Figure 2D displays glucose consumption. A blank without P38 was used for normalization, as mentioned in Table S4, which also contains the Supporting Information for Figure 2.

treated MIN6 cells with concentrations ranging from 0 to 1000 nM P38 to evaluate its impact on insulin secretion. The results, as depicted in Figure 2A, were obtained under the conditions of equilibration with 2.8 mM glucose for 1 h, followed by exposure to 25 mM glucose with peptides in KRBH at pH 7.4 and 0.1% BSA for 30 min. We selected this duration of 30 min because pancreatic beta cells typically reach their peak in the second phase of insulin secretion after glucose stimulation. Notably, at a hyperglycemic concentration of 25 mM, P38 significantly enhanced insulin secretion, as reported in the literature previously,[32] with the most pronounced effect observed at approximately 1.9-fold higher secretion when treated with 100 nM of P38 compared to others. We used a blank (0 nM P38 at 25 mM glucose) for standardization only in the context of Figure 2. Therefore, we identified 100 nM P38 as the concentration that induced the highest insulin secretion. Additionally, as demonstrated in Figure 2B–D, we found that the levels of cellular proteins, supernatant proteins, and glucose consumption remained consistent. This led to the conclusion that 100 nM P38 effectively enhanced insulin secretion. Consequently, we proceeded with further experiments involving different concentrations of viral peptide CV1 while maintaining a fixed concentration of 100 nM P38.

Effect of CV1 in the Presence of P38. In continuation of our investigation, we maintained a constant concentration of 100 nM P38 with CV1. We aimed to investigate the effects of the CV1 peptide at various concentrations while keeping the P38 concentration constant. This investigation was conducted in KRBH, same as above with 2.8 mM hypoglycemic treatment followed by 25 mM of glucose. The rationale for this choice was to gain insight into the effect of CV1 in the presence of P38. The outcomes of these experiments are presented in Figure 3A, where we observed a notable increase in insulin secretion as we augmented the concentrations of the CV1 peptide. To ensure accurate comparisons and standardization, we used NC (negative control) as a reference. The most significant enhancement, peaking at a remarkable 1.7-fold increase, was noted when utilizing 100 nM CV1 peptide. Importantly, we carefully assessed other key parameters, including glucose consumption, supernatant proteins, and cellular proteins, as described in Figure 3B–D, and found that these remained consistent throughout the experiments. This intriguing set of observations leads us to consider the possibility of synergistic or competitive interactions between the CV1 peptide and P38, possibly in their binding to PAC1R. Therefore, further, we have compared the individual effects of CV1 and P38 for long- and short-term treatment.

Short-Term Insulin Secretion. We exposed cells to P38 and CV1 peptides for 30 min to evaluate their short-term effects on insulin secretion via PAC1R interaction. We treated cells with P38 and CV1 independently for 30 min at 25 mM glucose in KRBH after equilibration with the hypoglycemic condition for 1 h. Insulin secretion increased by a remarkable 3.6-fold in CV1-treated cells compared to those treated with P38, as depicted in Figure 4A. The most substantial increase in insulin secretion and decrease in cellular protein levels were observed in CV1-treated cells, as shown in Figure 4B. The results in Figure 4A demonstrate that CV1 significantly augments insulin secretion to the point where it affects total cellular protein levels. This suggests the possibility of viral

https://doi.org/10.1021/acsinfecdis.4c01025
ACS Infect. Dis. 2025, 11, 1167−1179

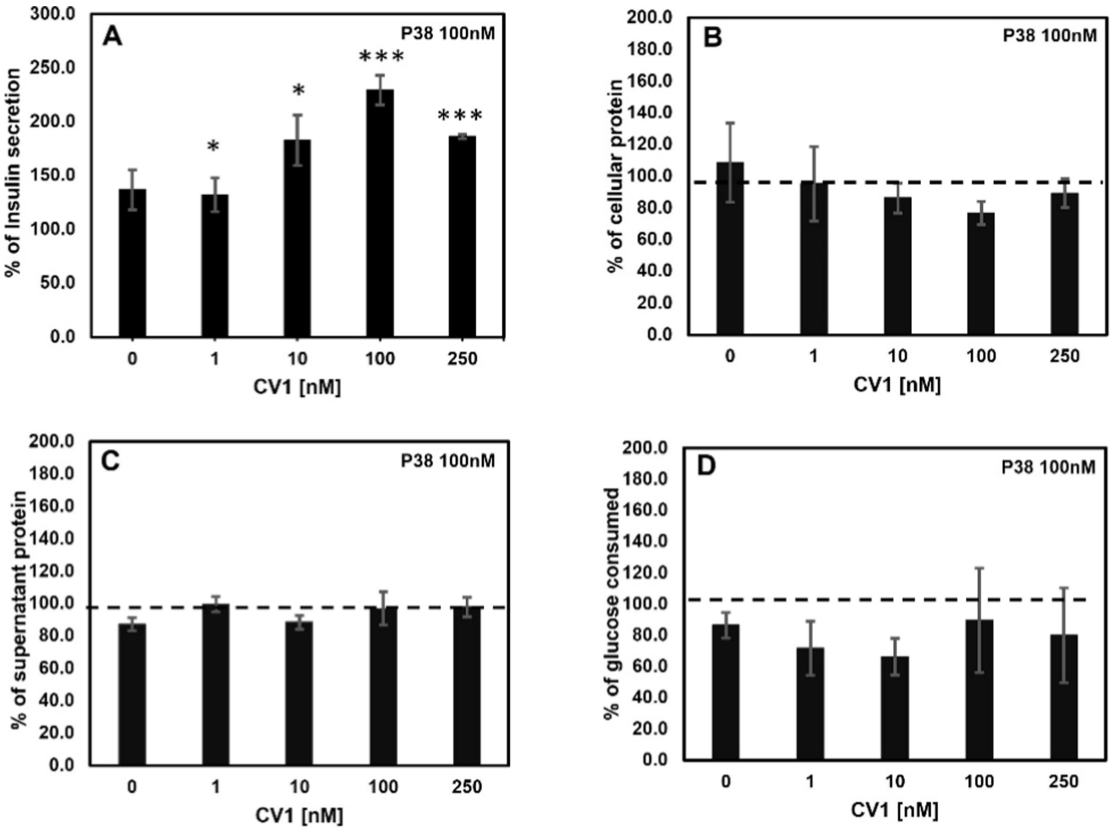

Figure 3. (A) Illustrates increasing insulin secretion as the concentration of CV1 viral peptide increases while maintaining a constant P38 concentration of 100 nM. The values represent SEM ± mean ($n = 3$), and p-values are denoted as * $p < 0.05$, ** $p < 0.01$, and *** $p < 0.001$, with P38 and NC serving as controls. Figure 3B and C displays cellular and supernatant proteins, and Figure 3D presents glucose consumption data. NC (negative control) is used as the standard for normalization, as mentioned in Table S5, which also contains the Supporting Information for Figure 3.

peptides outcompeting P38. CV1 has a significant effect on insulin secretion at 1 nM, suggesting a potent interaction with PAC1R, but its effect is minimal in the presence of P38, as shown in Figure 4A, likely due to competitive interactions or inhibition. Furthermore, CV1 treatment resulted in a decrease in total cellular proteins accompanied by an increase in insulin secretion, as illustrated in Figure 4B. Interestingly, supernatant proteins and glucose consumption levels remain unchanged, as depicted in Figure 4C and D. The significant reduction in cellular protein levels within 30 min of CV1 treatment could be due to a rapid stress response triggered by increased insulin secretion, resource reallocation toward insulin production, or heightened metabolic activity. It is conceivable that viral peptides stimulate insulin secretion to an extent that may negatively impact cellular health, potentially leading to either inhibition or a decrease in insulin secretion in the long term or rendering cells less responsive to glucose.

Long-Term Insulin Secretion. Next, we examined how cells maintain their GSIS after extreme insulin secretion. CV1-treated cells exhibit such a significant increase in insulin secretion that it raises concerns about its potential impact on pancreatic cell health. Cells must allocate energy resources for their survival, and long-term heightened secretion may compromise cellular functioning. To assess this, we subjected the cells to an extended treatment with peptides. We selected the following time intervals for long-term incubation because MIN6 cells duplicate during this time frame. It allows us to measure the effect of these peptides on insulin secretion from these cells, as expected in a biological system. First, we incubated these peptides for 24 to 48 h in serum-free media (SFM) to ensure that cellular health was maintained. Subsequently, we administered 25 mM of glucose treatment to assess the cellular response to hyperglycemia-induced insulin secretion after equilibrating at 2.8 mM of hypoglycemia in KRBH buffer with pH 7.4 and 0.1% BSA. The results, depicted in Figure 5A, demonstrate that cells treated with CV1 experience a 1.4-fold reduction in insulin secretion compared to those treated with P38. Cellular protein levels remained consistent in both P38- and CV1-treated cells across all concentrations. Importantly, there were no significant changes observed in cellular or supernatant proteins or glucose consumption, as illustrated in Figure 5B–D. The lack of significant change in cellular protein levels after 24 h of CV1 treatment in Figure 5B suggests cellular adaptation through homeostatic mechanisms, receptor downregulation, and compensatory synthesis pathways, reducing overstimulation of insulin secretion and normalizing protein levels. It is worth noting that no significant alterations were observed at the 48 h time point, as shown in Figure S1 and Table S10, respectively. The absence of significant changes at the 48 h time point implies that prolonged serum-free medium exposure might contribute to reduced cellular responsiveness to glucose, even in control cells. These findings suggest the possibility that prolonged exposure to CV1 may lead to a deprivation of insulin from the system and lead to a condition of T1D, characterized by cellular insensitivity to glucose.

https://doi.org/10.1021/acsinfecdis.4c01025
ACS Infect. Dis. 2025, 11, 1167−1179

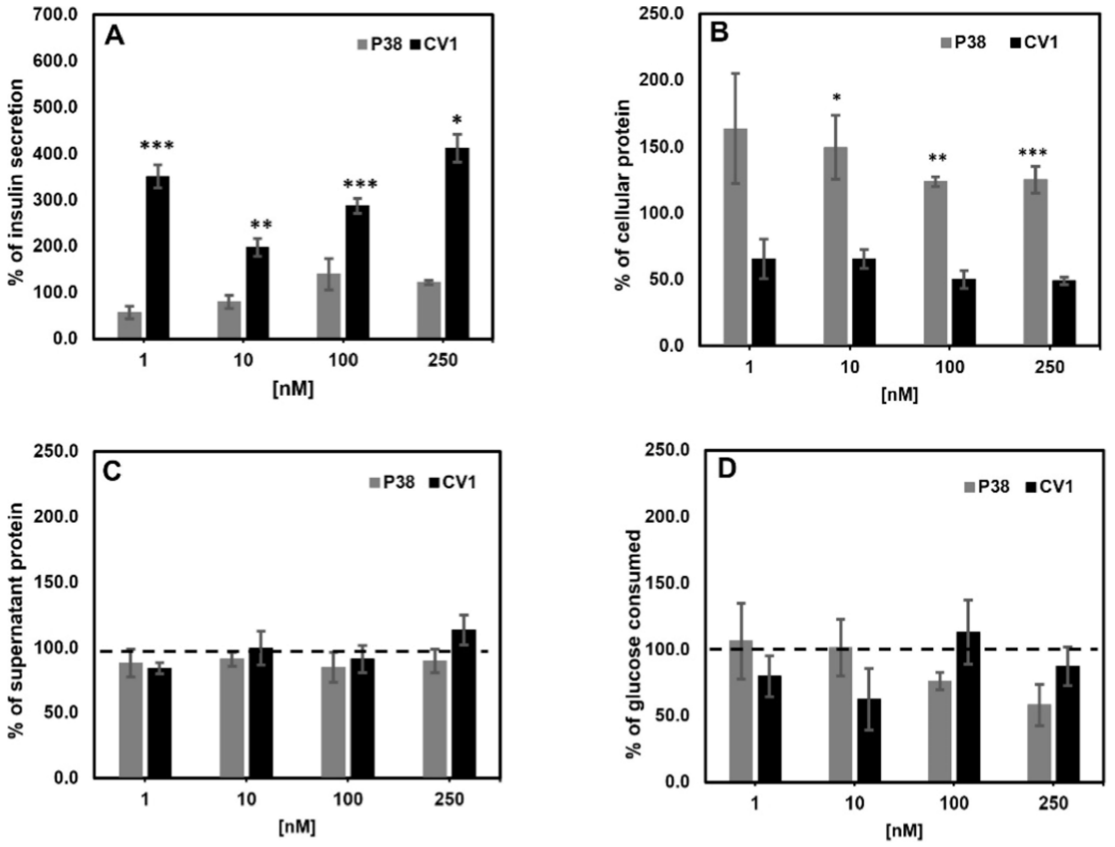

Figure 4. (A) Displays the most significant increase in insulin secretion when the concentration of CV1 is compared to P38 within a short treatment duration. In these graphs, the percentage of insulin secretion is calculated using NC as standard, as mentioned in Table S6. The values are presented as mean ± SEM (n = 3, triplicate), and significance is denoted by * $p < 0.05$, ** $p < 0.01$, and *** $p < 0.001$. Figure 4B demonstrates a substantial decrease in cellular protein in CV1-treated cells compared to P38, while Figure 4C and D illustrates changes in supernatant protein and glucose consumption. The Supporting Information for Figure 4 is provided in Table S6.

Cellular Viability after Short-Term and Long-Term Treatment. CV1 significantly boosts insulin secretion, affecting total cellular protein levels more than those of P38. Cells treated with CV1 show increased insulin levels but reduced protein levels, suggesting that high insulin secretion from viral peptides could harm cellular health. Assessing the cellular viability after peptide treatment is crucial. We employed the MTT assay to evaluate cell vitality for short- and long-term incubation; this cell viability assay was essential for proper interpretation of results from the MIN6 cellular model system. In Figure 6, it is evident that short-duration treatment with these peptides did not have any noticeable effect on cellular viability. We have examined the short-term treatment of peptides in both low and high passages to investigate the potential impact on cellular passage, as shown in Figure 6, panels A and B, while panel C presents the combined results of cellular viability. However, when it comes to long-term treatment with peptides, we generally did not observe any significant impact on cellular viability except under one condition. This becomes particularly significant under specific conditions, as when cells are exposed to 1 nM of peptides for 24 h, resulting in a noticeable difference in the percentage of cellular viability, as depicted in Figure 6D. While cellular viability shows recovery at 48 h, the initial drop likely reflects stress from viral peptides, potentially leading to adaptive responses and β-cell dysfunction over time, which aligns with Type 1 Diabetes mechanisms. Extended incubation data (for 72 h) are included in the Supporting Information as Figure S2, while ELISA (insulin assay) results are shown until 0−48 h. Insulin secretion assays were limited to 48 h due to experimental limitations, including those pertaining to health of cell cultures, the use of peptides and serum-free media, etc. In summary, we conducted these experiments to assess the effects of peptide treatment on cells at various passages, and while short-term treatments had no significant impact, longer-term exposure did reveal differences under certain conditions.

Investigating the Interactions of Peptides with PAC1R. Having established a clear functional role of viral peptide CV1, along with P38, in modulating insulin secretion by cells, it was important for us to investigate mechanisms of interaction(s) between the peptides and PAC1R. Ideally, it required us to purify PAC1R and determine interactive properties (e.g., dissociation constants) for CV1-PAC1R using P38-PAC1R as the positive control and NC-PAC1R as the negative control. However, we noted that the dissociation constant of the P38-PAC1R complex was reported in 1990 using membrane fractions derived from cells (rather than purified protein), as reviewed recently by Hirabayashi et al.[36] Further, the structure of P38-PAC1R (PDB ID: 6M1I) was reported only recently, i.e., 30 years subsequent to the above, by Wang et al.[33] Thus, realizing the nontrivial nature of obtaining wet-experimental insights into direct interactions of peptides with PAC1R to be beyond the scope of the current work, we carried out as-rigorous-as-possible computational investigation into these interactions by utilizing the recent 2024 Nobel-winning AlphaFold server. Specifically, we utilized

https://doi.org/10.1021/acsinfecdis.4c01025
ACS Infect. Dis. 2025, 11, 1167−1179

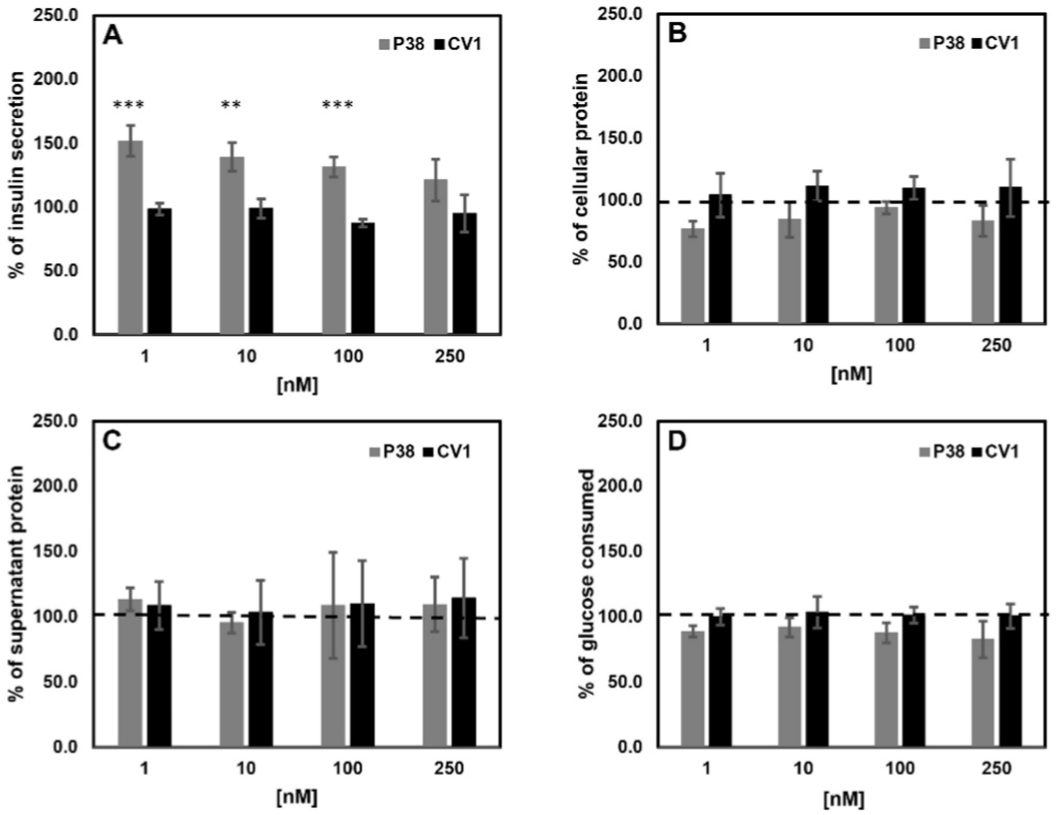

Figure 5. (A) Demonstrates a reduction in insulin secretion with an increasing concentration of CV1 compared to P38 after 24 h of long-term treatment. The values are presented as mean ± SEM (n = 4, triplicate), and significance is indicated by * $p < 0.05$, ** $p < 0.01$, and *** $p < 0.001$, using NC as a reference, as mentioned in Table S7 for 24 h treatment, and Table S10 for 48 h treatment. Figure 5B and C shows cellular and supernatant proteins, while Figure 5D displays glucose consumption, which remains consistent in both conditions. The Supporting Information for Figure 5 is provided in Table S7.

the AlphaFold 3 server, which can predict structures of peptide−protein complexes.[34,35] On feeding sequences of peptides and proteins, AlphaFold 3 provides structural output as five distinct models (called 0, 1, 2, 3, and 4, respectively, while specifically emphasizing that model "0" is the most reliable) based on different confidence metrics and accordingly assigns a "ranking score" (which is a function of free energy calculations) for each of the five models.[34,35] The most important aspect of this investigation was the availability of the P38-PAC1R complex structure, PDB ID: 6M1I—shown in Figure 7A, as a positive control and reference to benchmark the performance of AlphaFold 3 relevant to this work. Figure 7B, C, and E shows model "0" predicted by AlphaFold 3 for P38-PAC1R, CV1-PAC1R, and NC-PAC1R, respectively. Table S11 shows the remaining models 1, 2, 3, and 4 for the respective peptide-PAC1R complexes.

Having obtained P38-PAC1R structure predictions from AlphaFold 3, we first calculated the Root-Mean-Squared-Deviation (RMSD) of the predictions with PDB ID: 6M1I using the "align" function in PyMol. To our satisfaction, RMSD values for (a) all P38-PAC1R structures and (b) PAC1R structures alone (i.e., receptor structure postpeptide binding but without utilizing the peptide coordinates for RMSD calculations) were extremely low (0.801 to 1.056 Å), as shown in Table S12, thereby indicating the accuracy/reliability of AlphaFold 3 structural predictions; this can be noted visually also from Figure 7A vs 7B as well as Figure 7A vs column 2 of Table S11. Thus, the following results emerged:

1. AlphaFold 3 predicts the P38-PAC1R structure with high accuracy.
2. The CV1-PAC1R complex resembles P38-PAC1R but with distinct binding of the peptides in a nearby region of PAC1R—consistent with the observed nonlinear (including similar and sometimes synergistic) modulation of insulin secretion by CV1.
3. NC-PAC1R complex has nonspecific binding of the peptide at region distinct from P38 and CV1 with clear structural differences specifically at the original PAC1R region responsible for binding with P38 and CV1. Clearly, without affecting the overall structure of PAC1R, nonspecific binding of NC induces a conformational state characterized by the appearance of β-strands, quite different to the receptor's active conformational state required for proper downstream signaling. This is consistent with our observations of no role of NC binding on insulin secretion.

Based on the above information, the obvious next step was to investigate specific residues in PAC1R that were interacting with P38 and CV1. For this, the 2D diagram of P38-PAC1R and CV1-PAC1R complexes were visualized through BIOVIA Discovery Studio Visualizer 2025. As shown in Figure 7B−D and Figure S3, the peptide binding pockets of the PAC1R complex for bound P38 and CV1 peptides are distinct (but nearby). This was also evident from the involvement of different amino acid residues in H-bond formation within the receptor binding pocket of the PAC1R complex bound with P38 and CV1 peptides, as shown in Figure S4. Distinction of

https://doi.org/10.1021/acsinfecdis.4c01025
ACS Infect. Dis. 2025, 11, 1167−1179

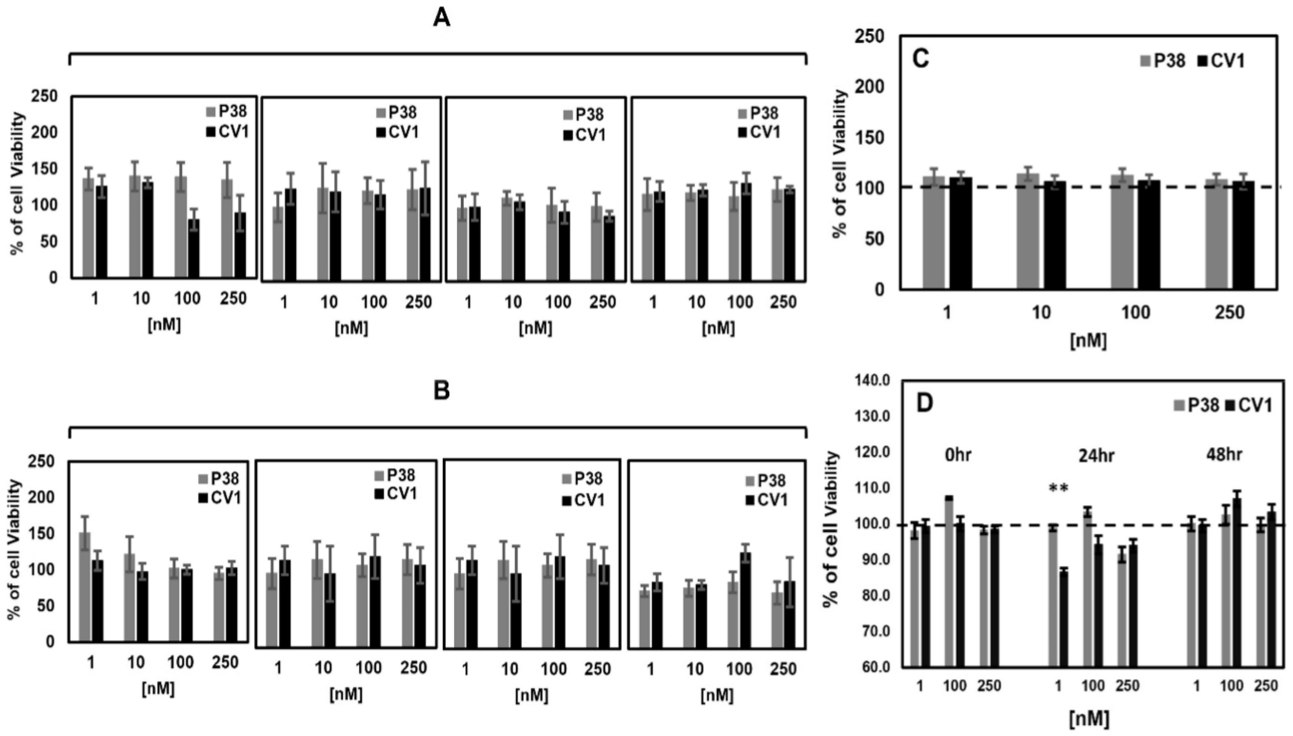

Figure 6. Panels (A) and (B) demonstrate cell viability at high and low passages after P38 and CV1 treatments, as assessed by the MTT assay for short-term treatment. Panel (C) displays the combined data for both lower and higher passage-treated cells, showing a 100% cell viability after treatment, with mean ± SEM (n = 7, triplicate). Panel (D) displays the percentage of cellular viability after P38 and CV treatment for long-term durations at 0, 24, and 48 h, with mean ± SEM (n = 8, triplicate). The Supporting Information for Figure 6 is provided in Tables S8 and S9.

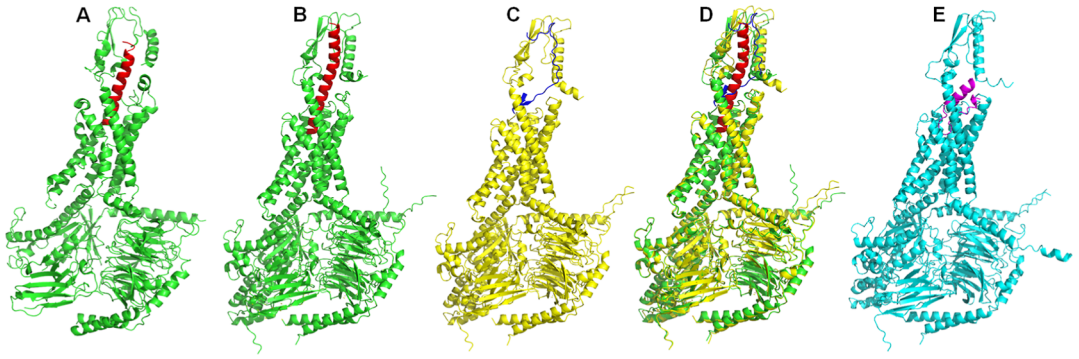

Figure 7. (A) Reported structure of the P38-PAC1R complex (PDB ID: 6M1I) with P38 shown in red, (B) AlphaFold 3-predicted model "0" for the P38-PAC1R complex, with P38 shown in red (RMSD = 0.839 Å when aligned with PDB ID: 6M1I using both P38 and PAC1R; RMSD = 0.838 Å for PAC1R only), (C) AlphaFold 3-predicted model "0" of the CV1-PAC1R complex, with CV1 shown in blue, (D) merged models of B and C showing that the CV1-PAC1R (CV1 in blue) complex resembles P38-PAC1R (P38 in red) but with distinct binding in a nearby region—consistent with the observed nonlinear modulation of insulin secretion by CV1, (E) NC-PAC1R complex, with NC shown in magenta showing (i) nonspecific binding of NC to PAC1R away from the "top region of activity" seen for P38 and CV1 and (ii) adoption of different structure of PAC1R in the presence of NC specifically with formation of new beta-strands at the "top region".

residues in binding to these peptides, with regional proximity, accounts well for the synergistic nonlinear response towards GSIS observed due to bound P38 and CV1 peptides within the PAC1R—these also suggest conformational plasticity of the peptide-PAC1R complex, especially in the presence of both the peptides. The lateral views of the obtained AlphaFold 3 model 0s of (B) P38-PAC1R complex, (C) CV1-PAC1R complex, and (D) the merged models (B and C) representing peptide-receptor binding pockets, along with the 2D interaction diagram of (B) and (C), are shown in the Supporting Information as Figures S3 and S4, respectively.

Calculating the Dissociation Constant (K_d) of the CV1-PAC1R Complex from Known K_d of P38-PAC1R Using Free-Energy-Based Scores of Predicted Structures

Having computationally demonstrated the potential binding of the viral peptide to PAC1R, the next step was to calculate equilibrium dissociation constants (K_d values) to ascertain differences in the affinities for the receptor. Detailed steps were followed to calculate the K_d for CV1-PAC1R from the known K_d of P38-PAC1R, and their respective ranking scores are provided in Table S13. Briefly, since (a) free energy is linearly added and subtracted and (b) the overall scores in predictive algorithms in AlphaFold 3 (as well as most other software

https://doi.org/10.1021/acsinfecdis.4c01025
ACS Infect. Dis. 2025, 11, 1167−1179

developed for structural predictions) are directly related/proportional to free energy calculations, a proportionality constant (α) between AlphaFold 3 ranking scores and free energy was assumed. Essentially, $\Delta G^\circ = \alpha$ x Score. Therefore, $-RT\ln(K_d) = \alpha$ x Score. Thus, if Score = 0.9 (for P38-PAC1R), and K_d = 0.5 nM, then $\alpha = [-2.48 \ln (5 \times 10^{-10})]/$ Score, i.e., α = 59.01. Therefore, for CV1-PAC1R, if Score = 0.86 and α = 59.01, then $K_d = e^{[\alpha \text{Score}/(-RT)]} \sim 1.3 \times 10^{-9}$ M = 1.3 nM.

Conclusions, Limitations of the Current Work, and the Way Forward. It would have been ideal to clone, express, and purify PAC1R protein and experimentally determine the interactive properties of the viral peptide CV1 with purified PAC1R, such as equilibrium dissociation constant (K_d) to ascertain differences in affinities for the receptor, using P38-PAC1R as a positive control and NC-PAC1R as a negative control. However, this work may take several more years, if it is limited to efforts only by our group, especially considering it took ∼30 years for structural information on P38-PAC1R subsequent to biochemical determination of the dissociation constant of this complex by utilization of cellular membrane fractions rather than purified PAC1R. Thus, we acknowledge that our work does not provide any wet-experimental biochemical evidence(s) for the direct interaction between CV1 and PAC1R and is currently limited to as-rigorous-as-possible computational evidence only. That said, the above does not dilute the fact that we have discovered and reported the first experimental evidence directly linking viral peptides to GSIS (specifically PACAP-stimulated), with functional assays reporting insulin secretion. This clearly opens new avenues for further research using viral-derived peptides. Additionally, our work establishes the first mechanistic connection between viral infections and the onset of Type 1 diabetes (T1D) that has been repeatedly observed in clinical literature without any possible direct correlation. In particular, our findings also support epidemiological reports associating acute chikungunya virus infection with subsequent diabetic ketoacidosis (DKA) in a patient with Type 1 diabetes.[12] It is our hope that our provocative findings will be found useful by the scientific community to overcome the aforementioned limitations collectively while expanding the scope of our findings on role of viral-peptides in GSIS, eventually building upon the strengths of our study, thereby fostering scientific advancement without compromising any rigor of proof.

Several studies have reported that the role of PACAP in regulating endocrine secretion in the pancreas is well established. Its immunoreactivity has been demonstrated in nerve fibers of intrapancreatic ganglia as well as in insulin-producing β-cells.[37] These cells also express PACAP receptors, PAC1R and VPAC2R, which bind with PACAP to activate adenylate cyclase and enhance GSIS.[38] Therefore, the abrogation of PACAP binding would inherently lead to unregulated insulin secretion and the dysregulation of glucose homeostasis. PACAP is known to upregulate the expression of selenoprotein T (SelT) in β-cells, which in turn caters to the feed-forward mechanism of prolonged insulin secretion.[39] This sustained release has been attributed to the antioxidant trait of SelT that maintains β-cell integrity by keeping a check on glucotoxicity developed by continuous insulin synthesis and secretion. Inactivation of the PACAP receptor signaling cascade would result in not only low insulin levels but also reduced β-cell numbers due to enhanced glucotoxicity of β-cells. The graphical abstract provides a comprehensive overview finding of our study. (A) demonstrates how P38 (PACAP) enhances insulin secretion in the presence of high glucose, aligning with the existing literature. Here, it is important to emphasize that while P38, being a peptide, is only a representative of full-length protein, it is established in the literature as the key fragment of the protein for interactions relevant to this work. Therefore, there is indeed a possibility of viral lytic fragments indulging in specific functionalities, especially under a high load of viral infection. In the presence of P38, the CV1-treated cell increases insulin secretion with an increasing glucose concentration. This shows that the CV1 peptide shows the highest similarity with P38 and can enhance the effect of PACAP-stimulated insulin secretion potentially. (B) highlights insulin secretion when CV1 is introduced alongside P38. When cells are treated with P38 and CV1 independently, it is interesting to note that CV1 outcompetes P38, enhancing insulin secretion in a short-term duration. This indicates that CV1 has a more pronounced effect on this specific receptor−ligand interaction. However, cellular protein is highly affected after CV1 treatment due to increased glucose-stimulated insulin secretion beyond a certain level. Decreased insulin secretion and reduction in β-cell mass in the virus-infected patient would mimic a T1D-like situation, as shown in (C) in short-term treatment. The results, indicating lower cellular protein levels with higher insulin secretion, suggest that CV1 peptides influence cellular proteins, potentially leading to an increase in insulin secretion, which could have long-term effects on the potency of insulin secretion. Of particular interest is the observation that these peptides, when subjected to short- or long-term treatments, do not display cellular cytotoxicity in most cases. However, certain conditions with CV1 peptides seem to result in long-term cytotoxicity. The rapid loss of cellular protein within 0.5 h of CV1 treatment, shown in Figure 4B, is likely due to a stress response and increased insulin production, and is not observed in the media (Figure 4C). Over time, as seen in Figures 3B,5B, and S1B, cells adapt and normalize protein levels. Figure 6 further shows that CV1 does not significantly affect cell health, indicating that the initial protein loss is transient. Furthermore, it is noteworthy that we observed a significant decrease in insulin secretion after long-term treatment with these CV1-treated peptides. The cells lose or reduce their sensitivity to glucose, and glucose no longer triggers GSIS potentiation under hyperglycemic conditions after CV1 peptide treatment. (D) reveals the impact of P38 and CV1 treatment on insulin secretion after long-term exposure to high glucose. Based on these findings, we concluded that viral peptides may play a significant role in precipitating a condition akin to T1D, wherein heightened insulin levels render cells unresponsive to hyperglycemic cues, subsequently impinging upon the intricate interplay between glucose sensitivity and PACAP-reinforced glucose-stimulated insulin secretion. While there is a substantial body of clinical evidence suggesting a connection between viral infections and T1D, these findings mark the first-ever studies that establish a mechanistic connection between viral infections and the initiation of the T1D condition. This widens the scope of the molecular mimics to act as a viral hormone capable of eliciting downstream signaling or a competitive inhibitor abrogating receptor function and calls for experiments on chemically synthesized viral peptides for validation. These findings not only add a novel dimension to the exploration of viral mechanisms for T1D induction but also

https://doi.org/10.1021/acsinfecdis.4c01025
ACS Infect. Dis. 2025, 11, 1167−1179

highlight the dependency of dynamic temporal patterns of T1D on this mechanism.

There are several explanations for emerging honeymoon phases reported in newly diagnosed T1D patients after being administered with exogenous insulin.[28,29] Increasing the production of specific proteins, such as insulin, can compromise the expression of other proteins, as suggested by secretory conservation in cellular secretion.[40] Viral infections alter PACAP signaling, leading to cell death and rendering the cells insensitive to glucose due to the metabolic burden caused by excessive insulin secretion. As cells regenerate, they become synchronized, resulting in an excessive production of insulin. However, their numbers remain insufficient to meet the insulin demand of the body. This excessive secretion may also cause metabolic burdens and cell death. Consequently, there is no honeymoon phase, and the system becomes dependent on external insulin for survival. This represents a timewise clinical manifestation that highlights the temporal nature of T1D. Future studies in this proposed direction are required to explore how these synchronized cells could potentially contribute to increased insulin production, which may offer potential benefits for diabetes treatment. However, this is to be tested experimentally. This hypothesis may offer insights into the broader spectrum of diabetes etiology and potentially open new avenues for the treatment and management of diabetes.

MATERIAL AND METHODS

It is important to emphasize that there is no use of human or animal samples or participants in this work. All work involves the use of standard biochemical and cell biology reagents only.

Chemicals. EZRMI-13K Insulin ELISA Assay Kit for rat/mouse, ethanol, and monosodium phosphate (NaH_2PO_4) were procured from Merck, USA. We obtained Dulbecco Modified Eagle's Medium (DMEM), fetal bovine serum (FBS), trypsin−EDTA, and PenStrep from Gibco, USA. Additionally, we sourced various supplies including glucose, potassium chloride (KCl), calcium chloride ($CaCl_2$), magnesium chloride ($MgCl_2$), monopotassium phosphate (KH_2PO_4), dipotassium phosphate (K_2HPO_4), HEPES, formaldehyde, sodium chloride (NaCl), sodium bicarbonate ($NaHCO_3$), 2-propanol, Bradford dye, and BSA from Himedia, India. *N*-Ethyl-*N*-sulfopropyl-*M*-toluidine, 4-aminoantipyrine, horseradish peroxidase, glucose oxidase, chloroform, and disodium phosphate (Na_2HPO_4) were acquired from Sigma, India. The peptides used in our study were custom synthesized by Gene Pro Biotech.

Data Collection and Sequence Alignment. Viral proteins from 5017 DV and 576 CHIKV complete genomes were downloaded from Virus Pathogen Research Database (www.viprbrc.org). Duplicate sequences were removed from the data to get a total of 3782 and 1497 unique DV and CHIKV sequences, respectively. Further, the data was imported to MATLAB (version R2017a), and the viral sequences were locally aligned against human P38. The alignments were screened to flag a continuous stretch of 4 identical residues, and the viral peptides exhibiting at least 50% coverage against P38 were selected for further analysis. Based on this criterion, two viral sequences aligned against human P38 were eliminated, while three DV and two CHIKV sequences were processed for the docking protocol.

Docking and Energy Calculations. *Docking.* Further, we tested the propensity of binding of the viral peptides with the PACAP-specific receptor, PAC1-R (Type 1 receptor). Before docking, the crystal structure of the extracellular domain of PAC1R (PDB ID: 3N94) was cleaned of heteroatoms and fusion protein (maltose-binding periplasmic protein) and subjected to energy minimization by Swiss-PDB Viewer 4.1.0. The five viral peptides screened from the above method were docked against the extracellular domain of PAC1R using the flexible protein-peptide docking protocol on CABS-Dock Web server for 100 simulation cycles.[30] Out of the two PACAP isoforms, P27 and P38, the latter is the more abundant form in pancreas[37] and PAC1R binds specifically to both with equal affinity.[41] Therefore, apart from P27, other variants of P38 were also considered for a positive control. Though the islet cells of the pancreas express both PAC1R and vasoactive intestinal peptide (VIP) receptor (VPAC2R), we restricted our binding studies to the former as it is PACAP-specific and has been known to bear a significant effect on insulin production in PAC1R-deficient mouse models.[38] Due to the restricted range of 4−30-mer peptides accepted by CABS-Dock, we could not dock P38 against PAC1R. Hence, to identify the control peptide, we sectioned P38 into 28-mer peptides comprising 11 peptides (1−28 *aa*, 2−29 *aa*, 3−30 *aa*, 4−31 *aa*, 5−32 *aa*, 6−33 *aa*, 7−34 *aa*, 8−35 *aa*, 9−36 *aa*, 10−37 *aa*, 11−38 *aa*). Since the viral peptides CV1, CV2, and DV2 also exceeded this range, the mismatched residues were trimmed from the ends to get suitable peptides (CV1: "FTDSRKISHTCTHPFHHEPPVIGRER"; CV2: "FTDSRKISHSCTHPFHHDPPVIGREKFH", and DV2: IFTTNIWLKLREKQDMICDSKLMSAAVK") for the docking protocol. Out of the 10 models predicted for each docking procedure, the one with the highest cluster density was selected for further analysis.

Molecular Dynamics and Binding Energy Calculations. Binding energy was calculated for each complex using the MM/PBSA protocol from the AMBER14 program package.[42,43] The best-predicted models for each of the PAC1R-peptide complex were further subjected to the *tleap* module to add counterions (Na^+/Cl^-) within the *ff99SB* force field, and the complex was immersed in a 12 A° *TIP3P* water box. Sander was used for molecular dynamics (MD) equilibrium, and the restraint was applied to the entire protein-peptide complex with 1000 cycles of steepest descent, 1000 cycles of conjugate gradient optimization. The system was heated from 0 to 300 K during 50 ps followed by 500 ps of equilibrium dynamics at *NPT* (P = 1 atm, T = 300 K). The simulations were set for a production step of 2 ns to give a total of 100 snapshots. Finally, *MM/PBSA.py* was executed for frames 5−100 to evaluate the binding free energy of the PAC1 receptor and peptide. Due to the predominance of negatively charged residues on the ligand binding domain of PAC1R,[31] this method was carried out at a higher solute dielectric constant (ε_{in} = 4).[44]

Identification of Potential Molecular Mimics of PACAP. Along with P27, the peptide-receptor complex with the highest binding affinity was selected as the positive control from the 28-mer variants of PACAP. The comparison of their binding free energy with that of the viral peptides helped to deduce the possibility of competitive binding between the PACAP variant and viral peptide. Finally, contact maps of the receptor-viral peptide complex with comparable binding affinities were obtained from CABS-dock results for assessment of the overlap in the binding interface of the receptor.

Cell Maintenance. We cultured MIN6 cells (Mouse Insulinoma 6) obtained from NCCS (National Centre for Cell Science, Pune, India) in DMEM with 25 mM glucose,

https://doi.org/10.1021/acsinfecdis.4c01025
ACS Infect. Dis. 2025, 11, 1167−1179

10% FBS, and 1% PenStrep, maintaining them at 37 °C with 5% CO_2.[26] Cells were kept healthy by changing the medium every other day and using cells with passage numbers under 30.

Insulin Secretion Assay. Standardization of P38. In a 24-well plate, cells were cultivated and seeded at a density of 2×10^5 cells per well, and they were used for experiments when they reached 75% confluency. Before experiments, cells were rinsed with Krebs Ringer Bicarbonate Buffer (pH 7.4) containing: KCl 4.7 mM, NaCl 119 mM, $CaCl_2$ 2.5 mM, $MgSO_4$ 1.2 mM, HEPES 10 mM, KH_2PO_4 1.19 mM, $NaHCO_3$ 20 mM, and 0.1% BSA. 0.1% BSA (1 mg/mL BSA) solution was included in the KRBH medium to stabilize the reaction, which may have masked other secreted proteins, but the analysis aimed to reflect the overall protein dynamics in the supernatant. In our experimental conditions, we used 2.8 mM glucose solely for the starvation phase across all experimental sets. Cells were equilibrated at 2.8 mM glucose for 1 h, then stimulated with 25 mM glucose and varying concentrations of P38 (0, 1, 10, 100, 1000 nM) or 250 nM negative control (NC) for 0.5 h in KRBH with 0.1% BSA, pH 7.4 at 37 °C and 5% CO_2,[26,45] After incubation, the cell supernatant was centrifuged at 2500 rpm for 5 min and stored at −20 °C for insulin and glucose assessment using the ELISA EZRMI-13K kit. Total cellular protein, normalized by the Bradford assay with BSA as the standard, was used for insulin analysis.

CV Treatment in the Presence of P38. Cells, maintained as described earlier, were washed twice upon reaching 75% confluence with KRBH. Subsequently, they were treated with 2.8 mM glucose for 1 h. CV treatments (1, 10, 100, and 250 nM) were carried out while maintaining a constant 100 nM P38 concentration, along with 25 mM glucose in KRBH with 0.1% BSA for 0.5 h at 37 °C and 5% CO_2. NC at 250 nM was included. Insulin, protein, and glucose assays were performed as previously described.

Long- and Short-Term Treatment. Cells were treated with P38 and CV at 1, 10, 100, and 250 nM, and NC at 250 nM, after equilibration with 2.8 mM glucose. Short-term treatments were in 25 mM glucose in KRBH with 0.1% BSA for 0.5 h at 37 °C and 5% CO_2, while long-term treatments were for 24, 48, and 72 h. Insulin, protein, and glucose levels were measured as described; the results are provided as bar diagrams instead of dose−response curves due to (a) absence of a continuous data and a continuous data analysis model and (b) to be able to compare individual bars for statistical significance.

Glucose Estimation. Residual glucose from the above experiments was collected and analyzed via an oxidase/peroxidase assay. The assay was carried out in a pH 6.0 80 mM sodium phosphate buffer (SPB) as per the protocol.[40,46]

Structure Prediction of Peptide-Receptor Complexes using AlphaFold 3 and Root-Mean-Squared-Deviation analyses, with PDB ID: 6M1I as Reference, Using PyMOL

The reported full-length structure of the P38-PAC1R complex (PDB ID: 6M1I)[33] was used as a reference structure; it was downloaded from the RCSB Protein Data Bank server (https://www.rcsb.org/). PAC1R sequence, utilized for the Cryo-EM structure, and respective peptide sequences (P38, CV1, and NC) were fed into AlphaFold server 3 (https://alphafoldserver.com/),[35] and the output models were downloaded containing the respective summary confidence JSON Files (.json), as well the Crystallographic Information Files (.cif). For RMSD analyses of the PAC1 receptor moiety post peptide binding (after removing the selected peptide atoms through the "action" command followed by the "remove atoms" command), .cif files of the peptide-receptor models 0−4 were aligned with the corresponding .cif files of peptide-receptor models 0−4 using the "align" command, respectively, through The PyMOL Molecular Graphics System, Version 3.1.3 Schrödinger, LLC. (https://www.pymol.org/#download), accessed on 24/01/2025, as mentioned in the Results and Discussion section and Table S12.

Visualization of Peptide Binding Pockets of PAC1R Complex through PyMOL and BIOVIA Discovery Studio Visualizer. The Crystallographic Information Files (.cif) of peptide-receptor model 0s obtained were viewed through PyMOL 3.1.3 software, as mentioned above. The peptide sequences (as ligands) were selected accordingly. To obtain the 2D diagram of the ligand binding site of model 0 peptide-receptor complex, the corresponding Crystallographic Information Files (.cif) of peptide-receptor model 0s was viewed through BIOVIA Discovery Studio Visualizer 2025 software (https://discover.3ds.com/discovery-studio-visualizer-download), accessed on 11/02/2025. The peptide sequence was selected as the ligand under "receptor−ligand interactions". Under "preferences", the ligand definition was increased to a 1000 atom limit, and subsequently, a force field was applied using the default "Apply Force field" function. The 2D diagram obtained of the ligand binding site of model 0 peptide-receptor complex was then saved as an .emf image file.

Calculation of the Dissociation Constant (K_d) for CV1 Binding to PAC1R. The summary confidence JSON Files (.json) of the respective model 0s contained the AlphaFold 3-predicted "ranking scores" for the corresponding peptide-receptor complex. Since (a) free energy is linearly added and subtracted and (b) the overall scores in predictive algorithms in AlphaFold 3 (as well as most other software developed for structural predictions) are directly related/proportional to free energy calculations, a proportionality constant (α) was calculated using the AlphaFold 3 ranking scores. Detailed steps followed to calculate the K_d for CV1-PAC1R from the known K_d of P38-PAC1R and their respective ranking scores are provided in Table S13.

Statistical Analysis. Statistical significance was assessed using a two-tailed Student's *t*-test in Excel 2016, with *p*-values below 0.05 considered significant.

■ ASSOCIATED CONTENT

Supporting Information

The Supporting Information is available free of charge at https://pubs.acs.org/doi/10.1021/acsinfecdis.4c01025.

Peptides and their sequences; binding free energy and disassociation constant of DV and CV peptides with PAC1R; residues of PAC1R binding to peptides; standardization of P38; effect of CV1 in the presence of P38; short-term insulin secretion (30 min); long-term insulin secretion (24 and 48 h); cellular viability after short-term treatment; cellular viability after long-term treatment; visualization of AlphaFold 3-predicted models (1−4) of different peptide-receptor complexes; RMSD analyses of AlphaFold 3-predicted structures aligned with the reference structure—PDB ID: 6M1I; visualization of peptide binding pockets of AlphaFold 3-predicted model 0 of the PAC1R complex bound with P38 and CV1 peptides; 2D diagram of the ligand binding site of model 0 peptide-receptor complexes; and

https://doi.org/10.1021/acsinfecdis.4c01025
ACS Infect. Dis. 2025, 11, 1167−1179

calculation of the dissociation constant (K_d) of CV1 with the PAC1R complex (PDF)

AUTHOR INFORMATION

Corresponding Author

Aditya Mittal − *Kusuma School of Biological Sciences, Indian Institute of Technology Delhi (IIT Delhi), New Delhi 110016, India;* orcid.org/0000-0002-4030-0951; Email: amittal@bioschool.iitd.ac.in

Authors

Firdos Firdos − *Kusuma School of Biological Sciences, Indian Institute of Technology Delhi (IIT Delhi), New Delhi 110016, India*

Tapabrata Pramanik − *Kusuma School of Biological Sciences, Indian Institute of Technology Delhi (IIT Delhi), New Delhi 110016, India*

Complete contact information is available at: https://pubs.acs.org/10.1021/acsinfecdis.4c01025

Author Contributions

†F.F. and T.P. contributed equally to the work. F.F. conceived the research, designed and performed the experiments, data analysis, and result interpretation, and wrote the manuscript. T.P. performed computational experiments and wrote the manuscript along with formatting and editing. A.M. conceived the research and contributed to data analysis, result interpretation, and manuscript writing and editing.

Funding

F.F. thanks the Council of Scientific and Industrial Research (CSIR) for providing fellowship support. T.P. is grateful to GATE-MoE, India, for providing fellowship support.

Notes

The authors declare no competing financial interest.

ACKNOWLEDGMENTS

F.F. thanks the Council of Scientific and Industrial Research (CSIR), India, for providing fellowship support. T.P. is grateful to GATE-MoE, India, for providing fellowship support. The authors also express gratitude to Dr. Manisha Priyam for her guidance in the initial project planning. A.M. acknowledges Siddhant Mittal for sharing clinical insights on Type 1 Diabetes and thanks Shweta Mittal and C.S. Dey for discussions that inspired research on cellular aspects of the disease.

REFERENCES

(1) Chiang, J. L.; Kirkman, M. S.; Laffel, L. M. B.; Peters, A. L. Type 1 Diabetes through the Life Span: A Position Statement of the American Diabetes Association. *Diabetes Care* **2014**, *37* (7), 2034−2054.

(2) Daneman, D. Type 1 Diabetes. *lancet* **2006**, *367* (9513), 847−858.

(3) Kollipara, S. Comorbidities Associated with Type 1 Diabetes. *NASN Sch. Nurse.* **2010**, *25* (1), 19−21.

(4) Principi, N.; Berioli, M. G.; Bianchini, S.; Esposito, S. Type 1 Diabetes and Viral Infections: What Is the Relationship? *J. Clin. Virol.* **2017**, *96*, 26−31.

(5) Yoon, J. W.; Austin, M.; Onodera, T.; Notkins, A. L. Virus-Induced Diabetes Mellitus: Isolation of a Virus from the Pancreas of a Child with Diabetic Ketoacidosis. *N. Engl. J. Med.* **1979**, *300* (21), 1173−1179.

(6) Dotta, F.; Censini, S.; Van Halteren, A. G. S.; Marselli, L.; Masini, M.; Dionisi, S.; Mosca, F.; Boggi, U.; Muda, A. O.; Prato, S. D.; Elliott, J. F.; Covacci, A.; Rappuoli, R.; Roep, B. O.; Marchetti, P. Coxsackie B4 Virus Infection of β Cells and Natural Killer Cell Insulitis in Recent-Onset Type 1 Diabetic Patients. *Proc. Natl. Acad. Sci. U.S.A.* **2007**, *104* (12), 5115−5120.

(7) Krogvold, L.; Edwin, B.; Buanes, T.; Frisk, G.; Skog, O.; Anagandula, M.; Korsgren, O.; Undlien, D.; Eike, M. C.; Richardson, S. J.; Leete, P.; Morgan, N. G.; Oikarinen, S.; Oikarinen, M.; Laiho, J. E.; Hyöty, H.; Ludvigsson, J.; Hanssen, K. F.; Dahl-Jørgensen, K. Detection of a Low-Grade Enteroviral Infection in the Islets of Langerhans of Living Patients Newly Diagnosed with Type 1 Diabetes. *Diabetes* **2015**, *64* (5), 1682−1687.

(8) Yeung, W. C. G.; Rawlinson, W. D.; Craig, M. E. Enterovirus Infection and Type 1 Diabetes Mellitus: Systematic Review and Meta-Analysis of Observational Molecular Studies. *Bmj* **2011**, *342*, d35.

(9) Economopoulou, A.; Dominguez, M.; Helynck, B.; Sissoko, D.; Wichmann, O.; Quenel, P.; Germonneau, P.; Quatresous, I. Atypical Chikungunya Virus Infections: Clinical Manifestations, Mortality and Risk Factors for Severe Disease during the 2005−2006 Outbreak on Réunion. *Epidemiol. Infect.* **2009**, *137* (4), 534−541.

(10) Lu, H. Z.; Xie, Y. Z.; Gao, C.; Wang, Y.; Liu, T. T.; Wu, X. Z.; Dai, F.; Wang, D. Q.; Deng, S. Q. Diabetes Mellitus as a Risk Factor for Severe Dengue Fever and West Nile Fever: A Metaanalysis. *PLoS Neglected Trop. Dis.* **2024**, *18* (5), No. e0012217.

(11) Kumar, S.; Lakhiwal, R.; Bhandiwad, C.; Chhimpa, A.; Gupta, A. Dengue Fever Presenting as Acute Pancreatitis. *Int. J. Res. Med. Sci.* **2017**, *5* (12), 5476.

(12) Tolokh, I.; Laux, T.; Kim, D. Case Report: A Case of Diabetic Ketoacidosis Following Chikungunya Virus Infection. *Am. J. Trop. Med. Hyg.* **2015**, *93* (2), 401−403.

(13) Fujinami, R. S.; Von Herrath, M. G.; Christen, U.; Whitton, J. L. Molecular Mimicry, Bystander Activation, or Viral Persistence: Infections and Autoimmune Disease. *Clin Microbiol Rev.* **2006**, *19* (1), 80−94.

(14) Ryu, W. S. Virus Life Cycle. *Molecular Virology of Human Pathogenic Viruses* **2017**, *31*, 31−45.

(15) Komatsu, M.; Takei, M.; Ishii, H.; Sato, Y. Glucose-Stimulated Insulin Secretion: A Newer Perspective. *J. Diabetes Investig* **2013**, *4* (6), 511−516.

(16) Firdos; Pramanik, T.; Verma, P.; Mittal, A. Re-Viewing Role of Intracellular Glucose Beyond Extracellular Regulation of Glucose-Stimulated Insulin Secretion by Pancreatic Cells. *ACS Omega* **2024**, *9* (10), 11755−11768.

(17) Thorens, B. Neuronal Glucose Sensing Mechanisms and Circuits in the Control of Insulin and Glucagon Secretion. *Physiol Rev.* **2024**, *104* (4), 1461−1486.

(18) Röder, P. V.; Wu, B.; Liu, Y.; Han, W. Pancreatic Regulation of Glucose Homeostasis. *Exp. Mol. Med.* **2016**, *48* (3), No. e219.

(19) Blad, C. C.; Tang, C.; Offermanns, S. G. Protein-Coupled Receptors for Energy Metabolites as New Therapeutic Targets. *Nat. Rev. Drug Discov* **2012**, *11* (8), 603−619.

(20) Morrow, J. A.; Lutz, E. M.; West, K. M.; Fink, G.; Harmar, A. J. Molecular Cloning and Expression of a CDNA Encoding a Receptor for Pituitary Adenylate Cyclase Activating Polypeptide (PACAP). *FEBS Lett.* **1993**, *329* (1−2), 99−105.

(21) Vaudry, D.; Falluel-Morel, A.; Bourgault, S.; Basille, M.; Burel, D.; Wurtz, O.; Fournier, A.; Chow, B. K. C.; Hashimoto, H.; Galas, L.; Vaudry, H. Pituitary Adenylate Cyclase-Activating Polypeptide and Its Receptors: 20 Years after the Discovery. *Pharmacol. Rev.* **2009**, *61* (3), 283−357.

(22) Sherwood, N. M.; Krueckl, S. L.; McRory, J. E. The Origin and Function of the Pituitary Adenylate Cyclase-Activating Polypeptide (PACAP)/Glucagon Superfamily. *Endocr Rev.* **2000**, *21* (6), 619−670.

(23) Goyal, D.; Pisegna, J. R. Pituitary Adenylate Cyclase-Activating Polypeptide. In *Pancreapedia: The Exocrine Pancreas Knowledge Base*, 2014.

(24) Yu, C. C.; Yang, C. Y.; Chang, T. Y.; Lan, K. C.; Liu, S. H. A Negative Regulatory Role of β-Cell-Derived Exosomes in the Glucose-

Stimulated Insulin Secretion of Recipient β-Cells. *Arch. Toxicol.* **2024**, *98*, 3885−3896.
(25) Miyazaki, J. I.; Araki, K.; Yamato, E.; Ikegami, H.; Asano, T.; Shibasaki, Y.; Oka, Y.; Yamamura, K. Establishment of a Pancreatic β Cell Line That Retains Glucose-Inducible Insulin Secretion: Special Reference to Expression of Glucose Transporter Isoforms. *Endocrinology* **1990**, *127*, 126−132.
(26) Ishihara, H.; Asano, T.; Tsukuda, K.; Katagiri, H.; Inukai, K.; Anai, M.; Kikuchi, M.; Yazaki, Y.; Miyazaki, J. I.; Oka, Y. Pancreatic Beta Cell Line MIN6 Exhibits Characteristics of Glucose Metabolism and Glucose-Stimulated Insulin Secretion Similar to Those of Normal Islets. *Diabetologia* **1993**, *36*, 1139−1145.
(27) Abdul-Rasoul, M.; Habib, H.; Al-Khouly, M. "The Honeymoon Phase" in Children with Type 1 Diabetes Mellitus: Frequency, Duration, and Influential Factors. *Pediatr Diabetes* **2006**, *7* (2), 101−107.
(28) Moole, H.; Moole, V.; Mamidipalli, A.; Dharmapuri, S.; Boddireddy, R.; Taneja, D.; Sfeir, H.; Gajula, S. Spontaneous Complete Remission of Type 1 Diabetes Mellitus in an Adult − Review and Case Report. *J. Community Hosp Intern Med. Perspect* **2015**, *5* (5), 28709.
(29) Li, S.; Fang, C.; Huang, Y.; Guo, H.; Hu, J. The Honeymoon Period Repeatedly Appears in Two Cases of Type 1 Diabetes Mellitus. *Acta Diabetol* **2017**, *54* (9), 877−880.
(30) Kurcinski, M.; Jamroz, M.; Blaszczyk, M.; Kolinski, A.; Kmiecik, S. CABS-Dock Web Server for the Flexible Docking of Peptides to Proteins without Prior Knowledge of the Binding Site. *Nucleic Acids Res.* **2015**, *43* (W1), W419−W424.
(31) Kumar, S.; Pioszak, A.; Zhang, C.; Swaminathan, K.; Xu, H. E. Crystal Structure of the PAC1R Extracellular Domain Unifies a Consensus Fold for Hormone Recognition by Class B G-Protein Coupled Receptors. *PLoS One* **2011**, *6* (5), No. e19682.
(32) Inagaki, N.; Yoshida, H.; Mizuta, M.; Mizuno, N.; Fujii, Y.; Gonoi, T.; Miyazaki, J. I.; Seino, S. Cloning and Functional Characterization of a Third Pituitary Adenylate Cyclase-Activating Polypeptide Receptor Subtype Expressed in Insulin- Secreting Cells. *Proc. Natl. Acad. Sci. U.S.A.* **1994**, *91* (7), 2679−2683.
(33) Wang, J.; Song, X.; Zhang, D.; Chen, X.; Li, X.; Sun, Y.; Li, C.; Song, Y.; Ding, Y.; Ren, R.; Harrington, E. H.; Hu, L. A.; Zhong, W.; Xu, C.; Huang, X.; Wang, H. W.; Ma, Y. Cryo-EM Structures of PAC1 Receptor Reveal Ligand Binding Mechanism. *Cell Res.* **2020**, *30* (5), 436−445.
(34) Jumper, J.; Evans, R.; Pritzel, A.; Green, T.; Figurnov, M.; Ronneberger, O.; Tunyasuvunakool, K.; Bates, R.; Žídek, A.; Potapenko, A.; Bridgland, A.; Meyer, C.; Kohl, S. A. A.; Ballard, A. J.; Cowie, A.; Romera-Paredes, B.; Nikolov, S.; Jain, R.; Adler, J.; Back, T.; Petersen, S.; Reiman, D.; Clancy, E.; Zielinski, M.; Steinegger, M.; Pacholska, M.; Berghammer, T.; Bodenstein, S.; Silver, D.; Vinyals, O.; Senior, A. W.; Kavukcuoglu, K.; Kohli, P.; Hassabis, D. Highly Accurate Protein Structure Prediction with AlphaFold. *Nature* **2021**, *596* (7873), 583−589.
(35) Abramson, J.; Adler, J.; Dunger, J.; Evans, R.; Green, T.; Pritzel, A.; Ronneberger, O.; Willmore, L.; Ballard, A. J.; Bambrick, J.; Bodenstein, S. W.; Evans, D. A.; Hung, C. C.; O'Neill, M.; Reiman, D.; Tunyasuvunakool, K.; Wu, Z.; Žemgulytė, A.; Arvaniti, E.; Beattie, C.; Bertolli, O.; Bridgland, A.; Cherepanov, A.; Congreve, M.; Cowen-Rivers, A. I.; Cowie, A.; Figurnov, M.; Fuchs, F. B.; Gladman, H.; Jain, R.; Khan, Y. A.; Low, C. M. R.; Perlin, K.; Potapenko, A.; Savy, P.; Singh, S.; Stecula, A.; Thillaisundaram, A.; Tong, C.; Yakneen, S.; Zhong, E. D.; Zielinski, M.; Žídek, A.; Bapst, V.; Kohli, P.; Jaderberg, M.; Hassabis, D.; Jumper, J. M. Accurate Structure Prediction of Biomolecular Interactions with AlphaFold 3. *Nature* **2024**, *630* (8016), 493−500.
(36) Hirabayashi, T.; Nakamachi, T.; Shioda, S. Discovery of PACAP and Its Receptors in the Brain. *J. Headache Pain* **2018**, *19* (1), 1−8.
(37) Filipsson, K.; Tornøe, K.; Holst, J.; Ahrén, B. Pituitary Adenylate Cyclase-Activating Polypeptide Stimulates Insulin and Glucagon Secretion in Humans. *J. Clin. Endocrinol. Metab.* **1997**, *82* (9), 3093−3098.
(38) Jamen, F.; Puech, R.; Bockaert, J.; Brabet, P.; Bertrand, G. Pituitary Adenylate Cyclase-Activating Polypeptide Receptors Mediating Insulin Secretion in Rodent Pancreatic Islets Are Coupled to Adenylate Cyclase but Not to PLC. *Endocrinology* **2002**, *143* (4), 1253−1259.
(39) Prevost, G.; Arabo, A.; Jian, L.; Quelennec, E.; Cartier, D.; Hassan, S.; Falluel-Morel, A.; Tanguy, Y.; Gargani, S.; Lihrmann, I.; Kerr-Conte, J.; Lefebvre, H.; Pattou, F.; Anouar, Y. The PACAP-Regulated Gene Selenoprotein T Is Abundantly Expressed in Mouse and Human β-Cells and Its Targeted Inactivation Impairs Glucose Tolerance. *Endocrinology* **2013**, *154* (10), 3796−3806.
(40) Firdos; Mittal, A. Secretory Conservation in Insulin Producing Cells: Is There a System- Level Law of Mass Action in Biology? *ACS Omega* **2023**, *8* (40), 37573−37583.
(41) Harmar, A. J.; Fahrenkrug, J.; Gozes, I.; Laburthe, M.; May, V.; Pisegna, J. R.; Vaudry, D.; Vaudry, H.; Waschek, J. A.; Said, S. I. Pharmacology and Functions of Receptors for Vasoactive Intestinal Peptide and Pituitary Adenylate Cyclase-Activating Polypeptide: IUPHAR Review 1. *Br. J. Pharmacol.* **2012**, *166* (1), 4−17.
(42) Miller, B. R.; McGee Jr, T. D.; Swails, J. M.; Homeyer, N.; Gohlke, H.; Roitberg, A. E. MMPBSA.Py: An Efficient Program for End-State Free Energy Calculations. *J. Chem. Theory Comput.* **2012**, *8* (9), 3314−3321.
(43) Case, D. A.; Babin, V.; Berryman, J. T.; Betz, R. M.; Cai, Q.; Cerutti, D. S.; Cheatham, T. E., III.; Darden, T. A.; Duke, R. E.; Gohlke, H.; Goetz, A. W.; Gusarov, S.; Homeyer, N.; Janowski, P.; Kaus, J.; Kolossváry, I.; Kovalenko, A.; Lee, T. S.; LeGrand, S.; Luchko, T.; Luo, R.; Madej, B.; Merz, K. M.; Paesani, F.; Roe, D. R.; Roitberg, A.; Sagui, C.; Salomon-Ferrer, R.; Seabra, G.; Simmerling, C. L.; Smith, W.; Swails, J.; Walker, R. C.; Wang, J.; Wolf, R. M.; Wu, X.; Kollman, P. A. *AMBER 14*; University of California: San Francisco, 2014.
(44) Hou, T.; Wang, J.; Li, Y.; Wang, W. Assessing the Performance of the MM/PBSA and MM/GBSA Methods. 1. The Accuracy of Binding Free Energy Calculations Based on Molecular Dynamics Simulations. *J. Chem. Inf. Model.* **2011**, *51* (1), 69−82.
(45) O'Driscoll, L.; Gammell, P.; Clynes, M. Mechanisms Associated with Loss of Glucose Responsiveness in Beta Cells. *Transplant. Proc.* **2004**, *36* (4), 1159−1162.
(46) Blake, D. A.; McLean, N. V. A Colorimetric Assay for the Measurement of D-Glucose Consumption by Cultured Cells. *Anal. Biochem.* **1989**, *177* (1), 156−160.

https://doi.org/10.1021/acsinfecdis.4c01025
ACS Infect. Dis. 2025, 11, 1167−1179

Supporting Information

Temporal effects of a viral peptide on glucose stimulated insulin secretion

Firdos Firdos[1@], Tapabrata Pramanik[1@] and Aditya Mittal[1*]

[1]Kusuma School of Biological Sciences, Indian Institute of Technology Delhi (IIT Delhi), Hauz Khas, New Delhi, 110016, India

*Correspondence: amittal@bioschool.iitd.ac.in

@ These authors contributed equally to the work

Number of pages: 21

Figures: 4

Tables: 13

Table of Contents:

Supplementary Table S1: Peptides and Their Sequences

P27	PACAP27
P38*	PACAP38
DV1	NS3 DEXDC domain (1675-1692)
DV2	NS1 (936-967)
DV3	NS5 (2862-2884)
CV1*	E2 (440-469)
CV2	E2 (440-472)
NC*	p130 (715-744)

NC: The Chikungunya virus structural polyprotein serves as the negative control peptide.
***Peptides were used for wet experiments based on their alignment and binding affinities with PAC1R.**

P38 HSDGIFTDSYSRYRKQMAVKKYLAAVLGKRYKQRVKNK

CV1 FTDSRKISHTCTHPFHHEPPVIGRERFHSR

NC MCARRRCITPYELTPGATVPFLLSLICCIR

Supplementary Table S2: Supporting information for Table 2: Binding free energy and disassociation constant of DV and CV peptides with PAC1R

First references 1-27 aa *	Binding Energy (Kcal/mol)	del-delG (kcal/mol)	Cal	Kdr/Kd'x'
DV1	-17.046	11.901	20.1712	5.76E+08
DV2	-36.6392	-7.6922	-13.038	2.18E-06
DV3	-34.1693	-5.2223	-8.8514	1.43E-04
CV1	-40.8629	-11.9159	-20.196	1.69E-09
CV2	-19.3724	9.5746	16.2281	1.12E+07
Second references 10-37 aa *				
DV1	-17.046	26.8293	45.4734	5.61E+19
DV2	-36.6392	7.2361	12.2646	2.12E+05
DV3	-34.1693	9.706	16.4508	1.39E+07
CV1	-40.8629	3.0124	5.10576	1.65E+02
CV2	-19.3724	24.5029	41.5303	1.09E+18

Supplementary Table S3: Residues of PAC1R binding to peptides

P38	P27	CV1
ARG A 95	ASN A 60	ALA A 41
ASN A 60	ASP A 59	ASN A 42
ASP A 100	CYS A 54	ASP A 100
ASP A 59	GLN A 31	ASP A 49
CYS A 113	GLU A 104	ASP A 59
CYS A 54	GLY A 56	CYS A 54
GLU A 104	ILE A 38	GLU A 104
GLY A 101	ILE A 61	GLY A 101
GLY A 114	ILE A 83	GLY A 46
ILE A 83	LEU A 35	GLY A 53
LEU A 35	LEU A 80	GLY A 56
MET A 57	LYS A 28	HIS A 108
PHE A 110	MET A 57	ILE A 38
PHE A 81	PHE A 27	MET A 45
PHE A 84	PHE A 81	MET A 57
PRO A 105	PRO A 55	PRO A 105
PRO A 55	TRP A 102	PRO A 52
TRP A 102	TRP A 58	PRO A 55
TRP A 58	TRP A 64	PRO A 66
TRP A 64	TYR A 109	SER A 103
TYR A 109		SER A 50
		SER A 51
		SER A 51
		TRP A 58
		TRP A 64

Supplementary Table S4: Supporting information for Figure 2: Standardization of P38 was done using blank values of 0 nM P38 which was used to express percent change in insulin secretion, the absolute value for insulin ELISA being 69.7 pmol/mg of insulin which correspond to a 100% level of insulin secretion.

% of insulin secretion					**% of cellular protein**			
Figure 2a					**Figure 2b**			
P38	**n1**	**n2**	**n3**	**n4**	**n1**	**n2**	**n3**	**n4**
1 nM	133.9	84.4	89.8	129.1	89.0	112.0	71.5	84.8
10 nM	172.8	72.5	132.4	152.9	65.4	126.9	73.3	76.6
100 nM	193.4	174.2	170.2	260.2	66.0	108.4	81.1	84.0
1000 nM			128.6	141.0		86.7	92.4	71.1
% of supernatant protein					**% of glucose estimation**			
Figure 2c					**Figure 2d**			
P38	**n1**	**n2**	**n3**	**n4**	**n1**	**n2**	**n3**	**n4**
1 nM	117.11	153.10	81.26	78.96	108.90	120.24	117.62	136.62
10 nM	124.28	67.78	93.29	81.66	97.81	73.81	105.27	85.75
100 nM	117.52	102.53	83.47	82.88	80.30	95.61	85.30	126.91
1000 nM			81.66	87.61	105.45	112.18	105.80	38.81

Supplementary Table S5: Supporting information for Figure 3: Effect of CV1 in presence of P38. Effect of CV1 in presence of P38: Standardization was done using the values of NC 250 nM which was used to express percent change in insulin secretion, the absolute value for insulin ELISA being 47.2 pmol/mg of insulin which correspond to a 100% level of insulin secretion.

% of insulin secretion				**% of cellular protein**		
Figure 3a				**Figure 3b**		
CV1	**a**	**b**	**c**	**a**	**b**	**c**
0 nM	101.6	163.7	144.8	133.86	84.15	107.60
1 nM	102.3	153.6	140.4	120.73	74.68	89.96
10 nM	144.6	177.9	225.6	96.63	78.12	83.93
100 nM	231.9	204.8	252.3	84.15	76.61	69.73
250 nM	183.1	190.2	186.4	88.24	98.57	80.70
Figure 3c				**Figure 3d**		
% of supernatant protein				**% of glucose estimation**		
CV1	**a**	**b**	**c**	**a**	**b**	**c**
0 nM	89.01	82.49	90.10	79.71	84.08	95.47
1 nM	94.20	101.45	102.78	78.99	84.32	51.75
10 nM	84.66	93.00	87.68	77.37	54.01	67.27
100 nM	105.19	85.27	100.12	111.15	106.47	51.18
250 nM	96.14	104.59	93.00	64.92	60.15	115.03

Supplementary Table S6: Supporting information for Figure 4: Short-term insulin secretion (30 minutes): Standardization was done using the values of NC 250 nM which was used to express percent change in insulin secretion, the absolute value for insulin ELISA being 51.41 pmol/mg of insulin which correspond to a 100% level of insulin secretion.

% of insulin secretion				**% of cellular protein**		
Figure 4a				**Figure 4b**		
P38	**n1**	**n2**	**n3**	**n1**	**n2**	**n3**
1 nM	45.53	83.10	41.87	45.53	83.10	41.87
10 nM	63.30	107.86	68.61	63.30	107.86	68.61
100 nM	132.16	149.16	138.49	132.16	149.16	138.49
250 nM	68.82	97.64	199.73	68.82	97.64	199.73
CV	**n1**	**n2**	**n3**	**n1**	**n2**	**n3**
1 nM	329.0	401.62	323.14	329.0	401.62	323.14
10 nM	234.8	187.25	170.92	234.8	187.25	170.92
100 nM	234.7	290.23	339.41	234.7	290.23	339.41
250 nM	321.2	563.42	352.40	321.2	563.42	352.40
% of supernatant protein				**% of glucose estimation**		
Figure 4c				**Figure 4d**		
P38	**n1**	**n2**	**n3**	**n1**	**n2**	**n3**
1 nM	98.6	99.4	67.5	99.35	179.26	40.72
10 nM	102.3	86.9	85.0	75.26	161.60	67.62
100 nM	100.6	69.5	85.3	100.10	96.90	32.18
250 nM	89.0	82.6	98.5	91.35	70.22	13.12
CV	**n1**	**n2**	**n3**	**n1**	**n2**	**n3**
1 nM	89.2	75.5	88.4	53.01	123.08	63.56
10 nM	101.6	77.0	120.8	44.09	126.29	17.37
100 nM	103.7	68.3	101.9	146.02	118.97	74.46
250 nM	128.8	99.2	112.8	116.60	120.88	24.87

Supplementary Table S7: Supporting information for Figure 5: Long-term insulin secretion (24 hours): Standardization was done using the values of NC 250 nM which was used to express percent change in insulin secretion, the absolute value for insulin ELISA being 51.41 pmol/mg of insulin which correspond to a 100% level of insulin secretion.

% of insulin secretion						**% of cellular protein**			
Figure 5a						**Figure 5b**			
P38	**n1**	**n2**	**n3**	**n4**	**n5**	**n1**	**n2**	**n3**	**n4**
1 nM		187.91	126.40	139.10	154.20	78.397	80.365	81.160	67.194
10 nM	156.17	167.02	97.33	148.06	127.52	91.630	97.623	65.259	82.196
100 nM	131.42	150.02	113.23	107.15	103.63	95.613	92.305	99.212	87.658
250 nM		175.76	99.89	112.36	97.40	64.560	87.349	91.453	89.383
CV	**n1**	**n2**	**n3**	**n4**	**n5**	**n1**	**n2**	**n3**	**n4**
1 nM		92.42	87.14	104.52	109.72	110.336	116.720	111.011	77.965
10 nM	80.11	121.99	82.10	109.80	101.13	116.554	116.371	118.787	93.571
100 nM	75.94	92.29	85.93	95.92	88.20	108.178	108.300	122.317	99.923
250 nM		143.34	75.17	84.21	77.87	80.439	110.556	137.020	112.001
% of supernatant protein						**% of glucose estimation**			
Figure 5c						**Figure 5d**			
P38	**n1**	**n2**	**n3**	**n4**		**n1**	**n2**	**n3**	**n4**
1 nM	121.476	119.205	102.187	110.502		82.12	101.25	82.74	88.86
10 nM	88.915	88.580	100.733	103.395		74.48	101.05	86.51	106.43
100 nM	87.235	85.928	92.580	169.437		68.59	105.12	85.54	92.17
250 nM	115.835	113.986	79.389	128.359		71.63	108.01	102.76	48.30
CV	**n1**	**n2**	**n3**	**n4**		**n1**	**n2**	**n3**	**n4**
1 nM	111.726	109.943	84.060	128.406		92.14	104.12	88.12	116.18
10 nM	93.935	91.914	88.484	139.899		80.73	105.23	91.78	136.28
100 nM	140.080	113.049	63.683	123.432		95.58	102.55	89.35	117.54
250 nM	115.077	118.262	75.408	149.434		84.08	114.39	85.24	118.73

Supplementary Table S8: Supporting information for Figure 6: Cellular viability after short term treatment

Figure 6a							
% of Cell viability							
n1							
P38	**A**	**B**	**C**	**D**	**E**	**F**	**G**
1 nM	106.156	130.416	138.508	141.684	135.274	150.136	151.357
10 nM	122.296	114.736	146.945	156.459	150.912	165.787	121.275
100 nM	112.336	120.313	108.685	159.952	147.606	163.991	160.297
250 nM	107.492	124.912	129.295	142.317	133.363	154.476	150.092
CV	**A**	**B**	**C**	**D**	**E**	**F**	**G**
1 nM	106.314	112.250	118.861	130.316	141.469	149.129	123.086
10 nM	125.372	124.955	129.080	134.570	145.306	131.911	127.355
100 nM	107.305	118.171	76.462	80.802	53.408	65.898	60.997
250 nM	65.179	111.459	110.798	103.482	61.831	97.331	77.870
n2							
P38	**A**	**B**	**C**	**D**	**E**	**F**	**G**
1 nM	89.038	120.184	120.532	109.132	110.871	76.187	76.822
10 nM	149.153	79.800	134.760	142.410	148.307	77.457	156.774
100 nM	136.876	137.859	151.724	85.183	83.338	132.567	134.019
250 nm	126.051	82.053	82.114	160.705	142.591	136.740	143.589
CV	**A**	**B**	**C**	**D**	**E**	**F**	**G**
1 nM	107.393	114.530	118.582	150.590	152.344	136.589	99.909
10 nM	116.223	129.936	82.250	92.667	143.151	157.635	131.978
100 nM	132.870	125.552	146.885	141.563	145.479	70.033	62.776
250 nM	102.419	131.751	124.524	123.496	134.170	131.267	135.062
n3							
P38	**A**	**B**	**C**	**D**	**E**	**F**	**G**
1 nM	103.750	71.470	103.371	98.112	87.625	113.267	120.253
10 nM	105.265	107.569	99.309	119.708	115.207	118.511	126.452
100 nM	90.944	102.689	121.754	67.166	109.281	115.889	118.511
250 nM	78.578	118.071	99.991	59.437	114.116	118.116	122.375
CV	**A**	**B**	**C**	**D**	**E**	**F**	**G**
1 nM	75.592	75.986	118.526	113.813	106.144	111.994	106.311

10 nM	90.141	100.628	115.889	105.690	111.069	117.237	114.616
100 nM	86.125	93.551	86.110	100.416	99.900	101.295	91.641
250 nM	68.075	83.518	91.489	90.080	100.294	104.674	83.867
n4							
P38	**A**	**B**	**C**	**D**	**E**	**F**	**G**
1 nM	89.323	129.494	139.566	100.521	97.405	134.447	135.620
10 nM	107.726	104.681	130.501	119.244	129.992	127.894	123.771
100 nM	100.355	128.747	114.907	126.200	86.136	125.773	125.975
250 nM	107.608	132.196	141.308	105.356	120.228	128.285	139.116
CV	**A**	**B**	**C**	**D**	**E**	**F**	**G**
1 nM	109.551	119.197	127.195	118.675	127.112	146.178	105.380
10 nM	110.179	126.816	121.152	119.351	133.298	129.518	127.634
100 nM	132.196	125.216	133.689	137.137	131.046	133.760	139.507
250 nM	117.976	147.814	129.553	131.414	97.121	118.154	132.693

Figure 6b % of Cell viability

n1								
P38	**A**	**B**	**C**	**D**	**E**	**F**	**G**	**H**
1 nM	187.546	121.612	123.077	169.963	152.381	167.033	140.659	147.985
10 nM	101.099	92.308	99.634	121.612	121.612	130.403	162.637	145.055
100 nM	102.564	106.960	99.634	90.842	101.099	92.308	105.495	117.216
250 nM	109.890	98.168	87.912	87.912	89.377	106.960	86.447	93.773
CV	**A**	**B**	**C**	**D**	**E**	**F**	**G**	**H**
1 nM	117.216	105.495	117.216	104.029	104.029	115.751	98.168	140.659
10 nM	93.773	86.447	102.564	79.121	111.355	111.355	95.238	102.564
100 nM	102.564	89.377	93.773	106.960	114.286	98.168	90.842	108.425
250 nM	104.029	86.447	73.260	86.447	139.194	118.681	106.960	106.960
n2								
P38	**A**	**B**	**C**	**D**	**E**	**F**	**G**	
1 nM	95.801	99.533	135.303	80.249	80.249	87.869	113.841	
10 nM	133.748	150.389	102.955	143.701	92.846	101.711	93.779	
100 nM	116.174	99.222	93.313	148.523	120.218	100.778	91.602	
250 nM	116.952	90.358	97.512	148.367	122.706	106.065	140.902	
CV	**A**	**B**	**C**	**D**	**E**	**F**	**G**	
1 nM	100.778	99.844	100.156	150.078	130.793	122.240	112.442	
10 nM	38.103	116.796	94.401	127.527	131.571	59.409	124.106	
100 nM	95.645	154.432	147.278	119.751	130.793	97.978	104.199	
250 nM	116.019	84.292	112.442	143.546	96.423	143.079	73.872	
n3								
P38	**A**	**B**	**C**	**D**	**E**	**F**	**G**	**H**

1 nM	84.995	100.767	82.366	99.890	101.643	99.014	142.826	133.187
10 nM	77.108	68.346	106.900	110.405	79.737	104.272	83.242	111.281
100 nM	159.474	134.064	126.177	106.900	108.653	97.262	105.148	116.539
250 nM	101.643	101.643	92.004	92.004	81.490	83.242	76.232	113.034
CV	**A**	**B**	**C**	**D**	**E**	**F**	**G**	**H**
1 nM	77.108	75.356	84.995	77.108	97.262	90.252	101.643	116.539
10 nM	88.499	73.604	96.386	99.890	82.366	70.975	77.108	73.604
100 nM	80.613	82.366	80.613	96.386	72.727	77.108	88.499	72.727
250 nM	102.519	75.356	101.643	155.969	135.816	124.425	203.286	64.841
n4								
P38	**A**	**B**	**C**	**D**	**E**	**F**	**G**	
1 nM	71.866	77.425	69.881	79.807	91.322	74.248	72.263	
10 nM	85.366	74.248	102.836	76.234	71.469	76.234	76.234	
100 nM	80.601	74.248	106.410	77.822	96.086	75.440	108.395	
250 nM	81.792	72.660	82.189	67.102	68.690	62.734	82.984	
CV	**A**	**B**	**C**	**D**	**E**	**F**	**G**	
1	73.454	81.395	93.307	85.366	80.204	106.807	97.277	
10	77.028	80.601	81.792	91.322	92.910	83.381	87.351	
100	124.277	103.233	94.101	127.453	97.277	169.938	172.717	
250	86.954	85.366	81.792	92.116	87.748	102.836	84.572	

Fig 6c % of Cell viability

P38	**n1**	**n2**	**n3**	**n4**	**n5**	**n6**	**n7**	**n8**
1 nM	105.59	151.28	76.69	98.98	136.22	100.40	99.69	118.05
10 nM	92.66	121.79	80.37	117.02	139.77	126.95	113.15	120.54
100 nM	119.28	102.01	88.43	109.98	139.03	123.08	103.75	115.44
250 nM	92.66	95.05	74.02	117.55	134.56	124.83	101.53	124.87
CV	**n1**	**n2**	**n3**	**n4**	**n5**	**n6**	**n7**	**n8**
1 nM	90.03	112.82	88.26	116.62	125.92	125.71	101.20	121.90
10 nM	82.80	97.80	84.91	98.84	131.22	121.98	107.90	123.99
100 nM	81.38	100.55	127.00	121.44	80.43	117.88	94.15	133.22
250 nM	120.48	102.75	88.77	109.95	89.71	126.10	88.86	124.96

Supplementary Table S9: Supporting information for Figure 6D: Cellular viability after long term treatment (0 hr, 24 hr, 48 hr, respectively)

0 hr				
P38	**n1**	**n2**	**n3**	**n4**
1 nM	88.7	107.5	88.7	107.5
100 nM	108.9	105.6	108.9	105.6
250 nM	103.2	93.4	103.2	93.4
CV	**n1**	**n2**	**n3**	**n4**
1 nM	110.5	99.3	88.7	99.3
100 nM	108.5	91.7	108.9	91.7
250 nM	101.3	94.7	103.2	94.7
24 hr				
P38	**n1**	**n2**	**n3**	**n4**
1 nM	98.39	104.98	96.51	95.80
100 nM	94.21	106.47	107.44	105.35
250 nM	80.65	85.72	102.99	96.86
CV	**n1**	**n2**	**n3**	**n4**
1 nM	82.3	83.0	93.6	87.7
100 nM	81.8	100.4	108.2	86.9
250 nM	85.9	96.4	105.9	87.7
48 hr				
P38	**n1**	**n2**	**n3**	**n4**
1 nM	87.4	104.0	111.1	97.9
100 nM	88.1	99.1	105.5	117.8
250 nM	90.5	94.6	102.4	111.7
CV	**n1**	**n2**	**n3**	**n4**
1 nM	92.3	97.5	96.4	111.8
100 nM	101.2	114.5	95.1	117.5
250 nM	92.5	98.3	105.7	117.0

Supplementary Figure S1: Long-term insulin secretion (48 hours)

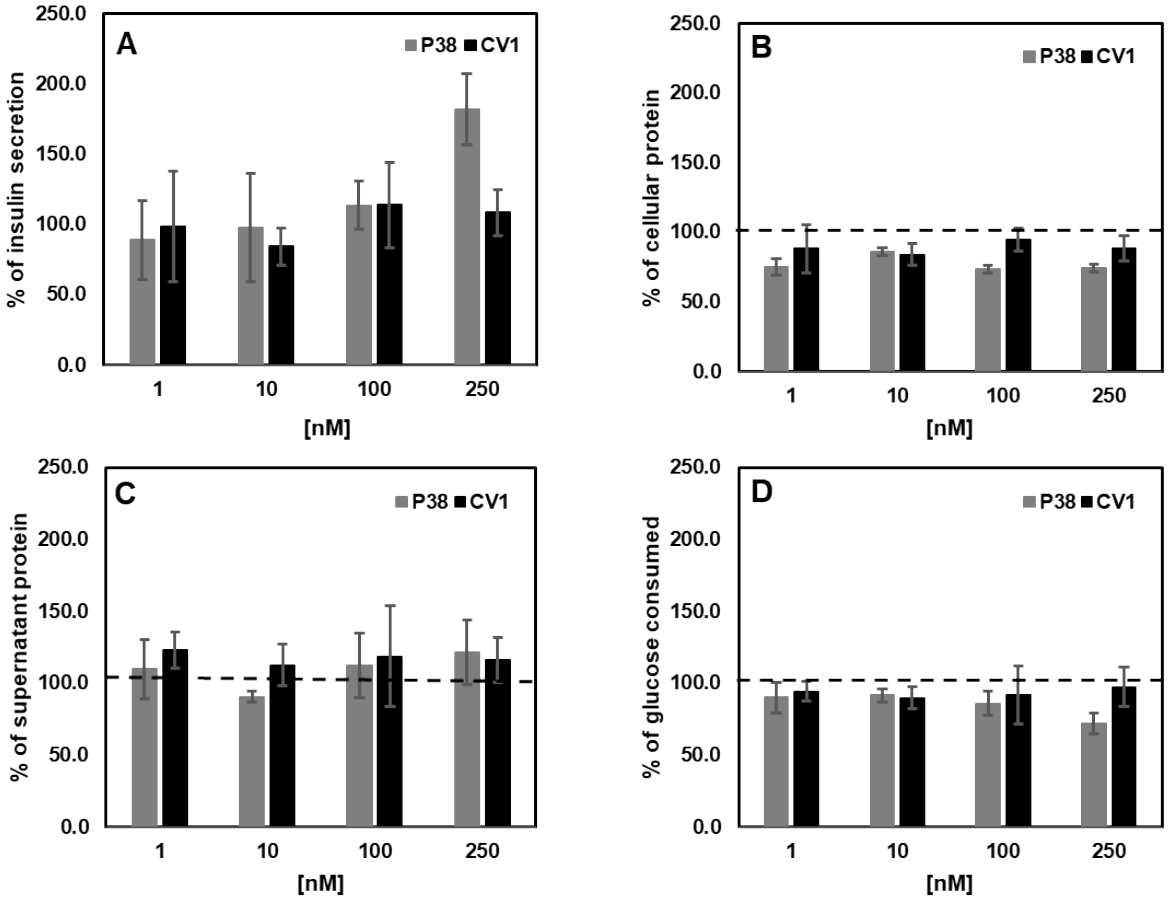

In Figure S1A, we observe an increase in insulin secretion in P38-treated cells at a concentration of 250 nM compared to CV1 after a 48-hour long-term incubation with peptides under glucose stimulation. The data is presented as Mean ± SEM (n = 3, with triplicate measurements), and statistical significance is denoted by * $p < 0.05$, ** $p < 0.01$, and *** $p < 0.001$, with NC used as a reference, as mentioned in supplementary table S10. Figures S1B and S1C depict cellular and supernatant proteins, and Figure S1D represents glucose consumption, which remains consistent in both experimental conditions.

Supplementary Table S10: Supporting information for Supplementary Figure S1: Long-term insulin secretion (48 hours): Standardization was done using the values of NC 250 nM which was used to express percent change in insulin secretion, the absolute value for insulin ELISA being 336.53 pmol/mg of insulin which correspond to a 100% level of insulin secretion.

% of insulin secretion				**% of cellular protein**		
Figure S1a				**Figure S1b**		
P38	**n1**	**n2**	**n3**	**n1**	**n2**	**n3**
1 nM	70.14	144.31	52.37	70.846	71.822	83.429
10 nM	89.58	168.31	35.61	61.163	73.166	124.646
100 nM	111.62	144.36	84.75	66.874	66.094	87.672
250 nM	143.71	230.33	171.57	57.814	78.670	86.783
CV	**n1**	**n2**	**n3**	**n1**	**n2**	**n3**
1 nM	76.94	174.57	44.14	68.458	96.003	100.659
10 nM	86.55	105.82	60.40	75.883	85.544	91.017
100 nM	57.64	161.54	122.19	90.369	89.503	104.721
250 nM	76.37	120.02	128.59	78.479	92.541	94.945
% of supernatant protein				**% of glucose estimation**		
Figure S1c				**Figure S1d**		
P38	**n1**	**n2**	**n3**	**n1**	**n2**	**n3**
1 nM	100.69	149.43	80.019	103.64	97.50	68.91
10 nM	86.16	88.08	97.687	94.68	97.29	82.93
100 nM	95.66	157.46	84.657	84.61	101.65	72.20
250 nM	108.56	165.34	90.564	64.23	86.35	64.81
CV	**n1**	**n2**	**n3**	**n1**	**n2**	**n3**
1 nM	126.97	142.06	100.068	101.23	101.46	80.33
10 nM	106.22	141.05	91.087	93.06	101.28	75.52
100 nM	88.32	188.35	79.570	127.18	92.02	56.74
250 nM	110.24	145.39	92.216	120.17	100.43	72.03

Supplementary Figure S2: Cellular viability after long term treatment (72 hours)

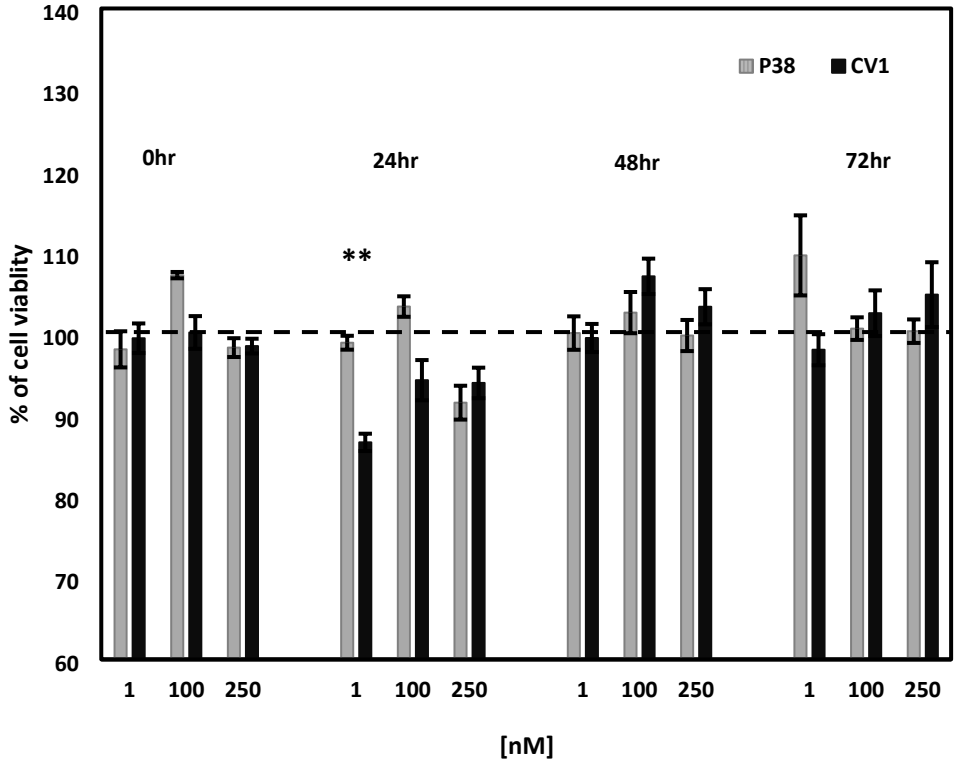

Supplementary Figure S2 displays the percentage of cellular viability after P38 and CV treatment for long-term duration till 72 hours, with Mean ± SEM (n = 8, triplicate) respectively. ELISA (insulin assay) results are shown till 0 hr - 48 hours.

Supplementary Table S11: Visualization of AlphaFold 3 predicted models (1-4) of different peptide-receptor complexes (Model 0 is shown in Fig. 7 of the main manuscript**)**

Model number	P38-PAC1R complex (P38 is marked in red)	CV1-PAC1R complex (CV1 is marked in blue)	Merged models	NC-PAC1R complex (NC is marked in magenta)
1.	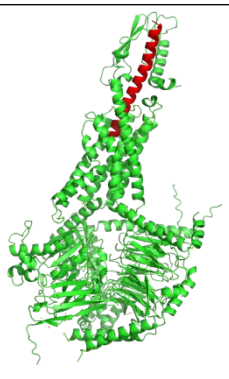		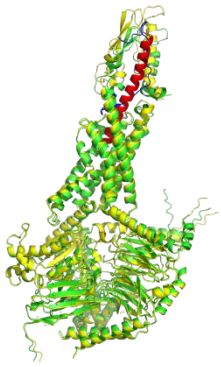	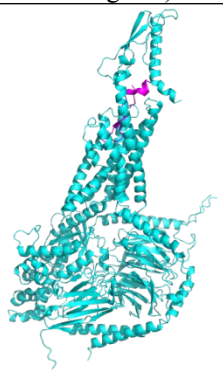
2.	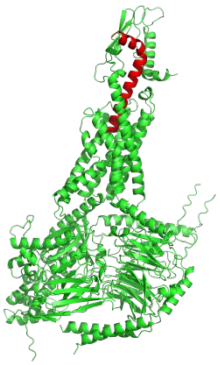	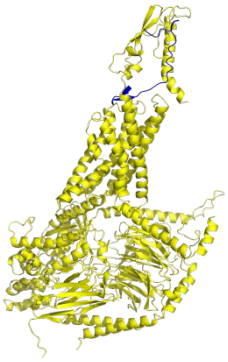	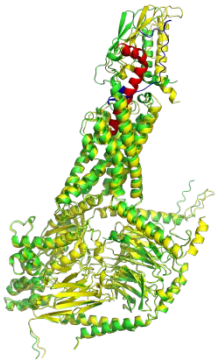	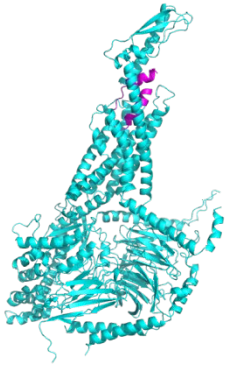
3.	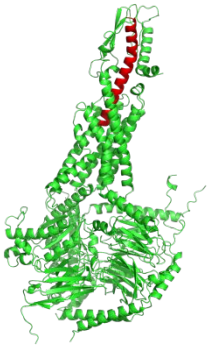	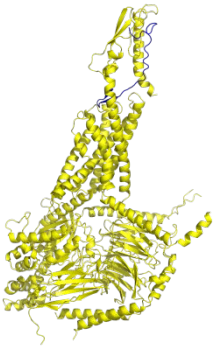	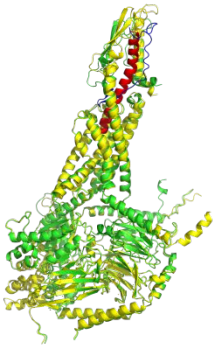	
4.	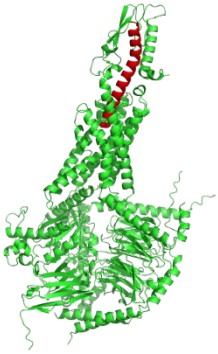	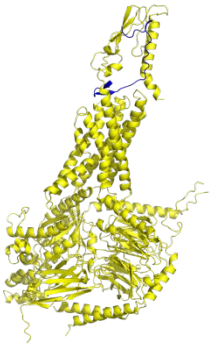	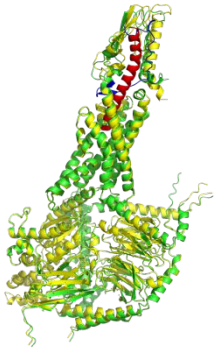	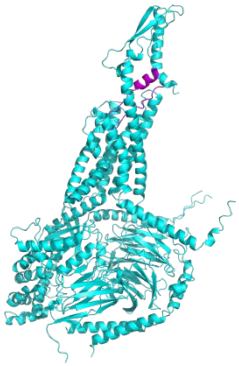

Supplementary Table S12: RMSD analyses of AlphaFold 3 predicted structures aligned with the reference structure - PDB ID: 6M1I

Comparison set	RMSD (Å)			
	P38-PAC1R complex vs the reference structure PDB ID: 6M1I	PAC1R (post P38 binding, without P38 atoms) vs the reference structure PDB ID: 6M1I (without P38 atoms)	PAC1R (post CV1 binding, without CV1 atoms) vs the reference structure PDB ID: 6M1I (without P38 atoms)	PAC1R (post NC binding, without NC atoms) vs the reference structure PDB ID: 6M1I (without P38 atoms)
model 0	0.839	0.838	0.804	0.843
model 1	1.03	1.013	0.836	0.902
model 2	0.951	0.94	0.899	0.866
model 3	0.807	0.801	0.95	1.056
model 4	1.016	0.995	0.997	0.906

Supplementary Figure S3: Visualization of peptide binding pockets of AlphaFold 3 predicted model 0 of PAC1R complex bound with P38 and CV1 peptides

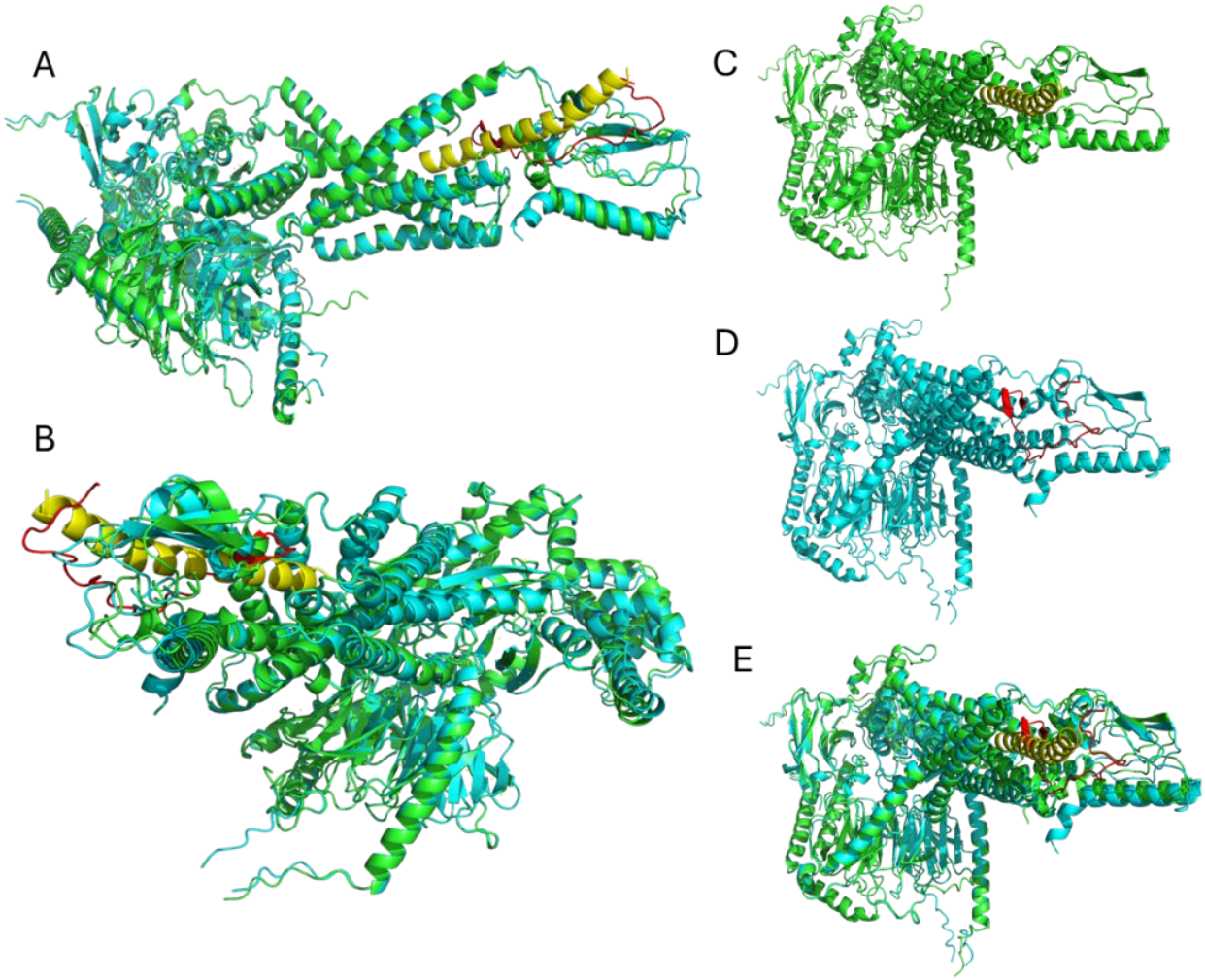

Figure S3 (A and B) displays lateral view of merged AlphaFold 3 peptide-receptor models. (C) lateral view of P38-PAC1R complex, (D) CV1-PAC1R complex and (E) merged models of C and D representing peptide-receptor binding pockets. P38 is marked in yellow and CV1 is marked in red, respectively.

Supplementary Figure S4: 2D diagram of the ligand binding site of model 0 peptide-receptor complexes

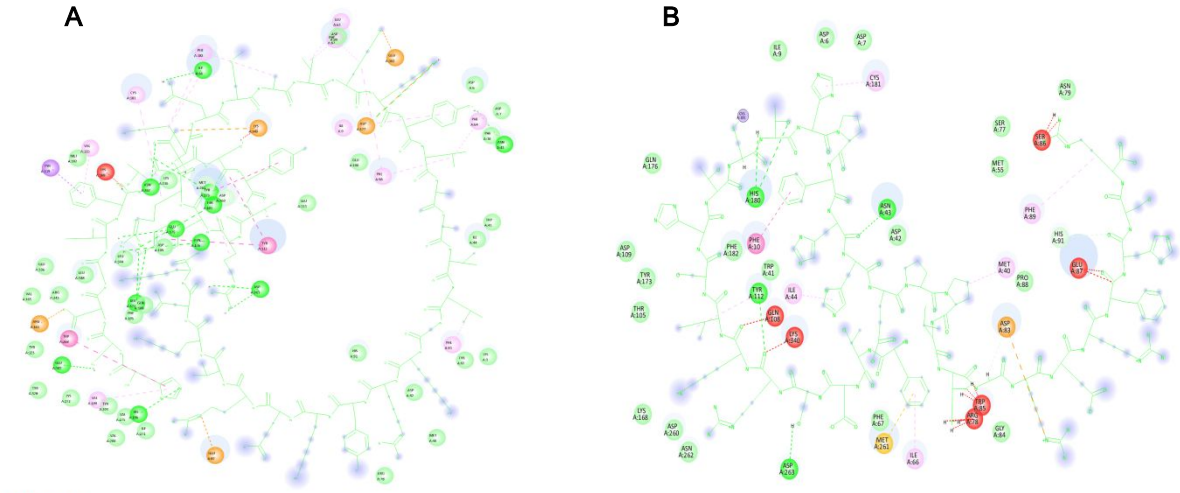

Figure S4 (A and B) displays the 2D diagram of corresponding ligand binding pockets of AlphaFold 3 predicted model 0's of (A) P38-PAC1R complex, and (B) CV1-PAC1R complex.

Supplementary Table S13: Calculation of dissociation constant (K_d) of CV1 with PAC1R complex

Step No.	Procedure
1	Consider $\Delta G° = -RTln(K_d)$. Since "Score" used by AlphaFold 3 (and generally all predictive software) is a function of free energy calculations, let us assume $\Delta G° = \alpha$ x Score, where "α" is a proportionality constant
2	Take the reported* K_d value of P38-PAC1R; This is 0.5 nM = $5x10^{-10}$ M
3	For calculation of "RT" in Step 1, R = 8.314 J/mol.K, T = 298 K; Therefore -RT ~ -2.48 KJ/mol
4	Calculate the value for $\Delta G°$ for K_d value of P38-PAC1R as $5x10^{-10}$ M
5	Calculate the value for "α" from Step 3 and Step 1 given the "Score" of P38-PAC1R by AlphaFold 3
6	Use the calculated value of "α" in Step 4, and the "Score" of CV1-PAC1R to calculate $\Delta G°$ for CV1-PAC1R
7	From $\Delta G°$ obtained for CV1-PAC1R in Step 6, calculate K_d for CV1-PAC1R

*From Reference No. 36 (a review by Hirabayashi et al., 2018 based on actual determination of binding constants using membrane fractions containing PAC1R in 1990)

Since (a) free energy is linearly added and subtracted, and (b) the overall scores in predictive algorithms in AlphaFold 3 (as well as most other software developed for structural predictions) are directly related/proportional to free energy calculations, a proportionality constant (α) was calculated using the AlphaFold 3 ranking scores. The above implies that $\Delta G° = \alpha$ x Score. Therefore, $-RTln(K_d) = \alpha$ x Score. Thus, if Score = 0.9 (for P38-PAC1R), and K_d = 0.5 nM, then $\alpha = [-2.48 \ln (5x10^{-10})]$/Score, i.e. $\alpha = 59.01$. Therefore, for CV1-PAC1R, if Score = 0.86 and $\alpha = 59.01$, then $K_d = e^{[\alpha Score/(-RT)]} \sim 1.3 \times 10^{-9}$ M = 1.3 nM.

It is important to note the following:

1. "Score" for output models 0, 1, 2, 3, 4 of P38-PAC1R were 0.90, 0.89, 0.89, 0.89, 0.89 respectively. As per instructions of AlphaFold 3, Model-0 score is most reliable.
2. "Score" for output models 0, 1, 2, 3, 4 of P38-PAC1R were 0.86, 0.86, 0.85, 0.85, 0.85 respectively. As per instructions of AlphaFold 3, Model-0 score is most reliable.